https://doi.org/10.5194/egusphere-2023-1816
Preprint. Discussion started: 18 August 2023

21st century marine climate projections for the NW European Shelf Seas based on a Perturbed Parameter Ensemble.

Jonathan Tinker[1], Matthew D. Palmer[1,2], Benjamin J. Harrison[1], Enda O'Dea[1,3], David M.H. Sexton[1], Kuniko Yamazaki[1], John W. Rostron[1]
[1]Met Office, Exeter, EX1 3PB, UK.
[2]School of Earth Sciences, University of Bristol, UK.
[3] Met Éireann, Dublin, D09 Y921, Ireland.

Correspondence to: Jonathan Tinker (jonathan.tinker@metoffice.gov.uk)

Abstract. The North West European Shelf Seas (NWS) are environmentally and economically important, and an understanding of how their climate may change helps with their management. However, as the NWS are poorly represented in Global Climate Models, a common approach is to dynamically downscale with an appropriate shelf seas model. We develop a set of physical marine climate projections for the NWS. We dynamically downscale 12 members of the HadGEM3-GC3.05 Perturbed Parameter Ensemble (approximately 70 km horizontal resolution over Europe), developed for UKCP18, using the shelf-seas model NEMO CO9 (7 km horizontal resolution). These are run under the high greenhouse gas emissions RCP8.5 scenario as continuous simulations over the period 1990-2098. We evaluate the simulations against observations in terms of tides, sea surface temperature, surface and near-bed temperature and salinity, and sea surface-height. These simulations represent the state-of-the-art for marine UK projections. We project a Sea-Surface Temperature (SST) rise of 3.11 °C ($\pm 2\sigma$ = 0.98 °C), and a Sea-Surface Salinity (SSS) freshening of −1.01 psu ($\pm 2\sigma$ = 0.93 psu) for 2079-2098 relative to 2000-2019, averaged over the NWS (approximately bounded by the 200m isobar and excluding the Norwegian Trench, Skagerrak, and Kattegat). While the patterns of NWS changes are similar to our previous projections, there is a greater warming and freshening, that could reflect the change from the A1B emissions scenario to the RCP8.5 concentrations pathway or the higher climate sensitivity exhibited by HadGEM3-GC3.05. Off the shelf, south of Iceland, there is limited warming, consistent with a reduction in the Atlantic Meridional Overturning Circulations and associated northward heat transport. These projections have been publicly released, along with a consistent 200-year present day control simulation, to provide an evidence-base for climate change assessments and to facilitate climate impact studies. For example, we illustrate how the two products can be used to estimate of climate trends, unforced variability, and the Time of Emergence (ToE) of the climate signals. We calculate the average NWS SST ToE to be 2034 (with an 8-year range) and 2046 (with a 33-year range) for SSS. We also discuss how these projections can be used to describe NWS conditions under 2°C and 4°C global mean warming (compared to 1850-1900), as a policy relevant exemplar use-case.

https://doi.org/10.5194/egusphere-2023-1816
Preprint. Discussion started: 18 August 2023

1 Introduction

The North West European Shelf Seas (NWS) are economically and environmentally important (Pugh, 2008; Tinker et al., 2018). They are quasi-isolated from, and behave differently to, the North Atlantic, and have a different response to climate change (Holt et al., 2010; Wakelin et al., 2009). They are generally poorly represented in Global Climate Models (GCMs) and global ocean models due to limited vertical and horizontal resolution and the absence of key processes, such as tides (Tinker et al., 2022). Therefore, assessing the NWS response to climate change directly from GCMs may be inappropriate for many applications (Hermans et al., 2020b; Tinker et al., 2022; Mathis et al., 2013). A common approach to mitigate these shortcomings is to dynamic downscale GCM climate projections with a higher resolution shelf seas model, which includes the additional relevant processes (e.g. Holt et al., 2010; Tinker et al., 2016, 2020).

The marine component (Palmer et al., 2018) of the recent national UK Climate projections, UKCP18 (Murphy et al., 2018), had a sea level focus (see their table 5.1). UKCP18 provided mean sea level projections (for the 21st century and exploratory extended projections to 2300) (Palmer et al., 2020), estimates of the change in the surge and wave climate (Howard et al., 2019), and a quantification of the present day sea level variability (Tinker et al., 2020). The climate projections of ocean water properties for the NWS from UKCP09 (Lowe et al., 2009) and the Minerva Projections (Tinker et al., 2015, 2016) were not updated in UKCP18. The UK's third Climate Change Risk Assessment (CCRA3) used UKCP18 as a primary source of evidence, however as the NWS climate projections had not been updated assessment of those aspects was based on the older UKCP09/Minerva NWS projections. As well as being based on outdated science, use of the earlier NWS projections may introduce inconsistencies with the wider CCRA3 findings based on UKCP18. With the evidence call for the upcoming 4th CCRA approaching, we have developed a set of NWS climate projections, based on, and consistent with the UKCP18 marine projections.

In this paper (and dataset) we downscale UKCP18 12-member Perturbed Parameter Ensemble (PPE), based HadGEM3-GC3.05, run under the RCP8.5 high emissions climate change scenario. The PPE simulations are downscaled with the shelf seas version of NEMO 4.04 (Coastal Ocean version 9, CO9), as transient simulations for the period 1990-2098. We use the methodology and evaluation developed by Tinker et al. (2020) to produce a set of projections consistent with their estimate of NWS unforced variability. These updated NWS climate projections (hereinafter NWSPPE) are released, with the present-day control simulation (hereinafter PDCtrl) of Tinker et al. (2020), in time for use in the UK's 4th CCRA.

https://doi.org/10.5194/egusphere-2023-1816
Preprint. Discussion started: 18 August 2023

2 Data

In this section we describe the datasets used in this study. Our simulations are driven by GCM model output, so we give a brief overview of the GCM (HadGEM3-GC3.05) and the data used – a detailed description of HadGEM3-GC3.05 and its evaluation for the NWS is given in Tinker et al. (2020). We also describe the observation data sets and the Copernicus Marine Service NWS Reanalysis used in our evaluation.

2.1 The HadGEM3-GC3.05 PPE

HadGEM3-GC3.05 (Williams et al., 2018; Yamazaki et al., 2021) is the Met Office GCM used in the 2018 UK Climate projections (UKCP18) and very similar to the model submitted to CMIP6 (Coupled Model Intercomparison Project Phase 6, Eyring et al., 2016). HadGEM3-GC3.05 is based on the Met Office Unified Model atmosphere (Walters et al., 2019) (with approximately 70km resolution of Europe) and the ocean model NEMO, run on the ORCA025 grid (~ 1/4° horizontal resolution on a tri-polar grid). HadGEM3-GC3.05 uses the CICE sea ice model (Hunke et al., 2015) with GSI8.0 science (Ridley et al., 2018) on the same ORCA025 grid. HadGEM3-GC3.05 does not simulate tides or other important shelf seas processes. HadGEM3-GC3.05 is run with a 360-day calendar, with 12 months of 30 days. This has little impact on the climate projections, but is not directly compatible with observed tides, which are constrained by astronomical frequencies. This discussed later.

We use HadGEM3-GC3.05 model output from the atmosphere and the ocean model to drive our downscaled shelf seas simulations. HadGEM3-GC3.05 atmospheric surface fluxes of heat, fresh water and momentum are used, as is ocean temperature, salinity, currents, and sea surface height from the HadGEM3-GC3.05 ocean. Tinker et al. (2020) lists all the HadGEM3-GC3.05 variables used to driver our simulation, and their frequency, in their Table S9.

2.2 Observational Datasets

We use several observational datasets to evaluation the NWSPPE. Tinker et al. (2020) evaluated PDCtrl, and we follow a similar approach here.

2.2.1 OSTIA

We use the OSTIA (Operational Sea-Surface Temperature and Sea-Ice Analysis) SST analysis product (Roberts-Jones et al., 2012) to evaluate the NWSPPE SST. OSTIA is a largely satellite-based SST dataset on a horizontal grid of 0.25° which we bi-linearly interpolated onto the AMM7 model grid. The OSTIA assimilates several bias corrected satellite products to reduce the bias of the overall product.

We calculate an SST climatology (mean and standard deviation) for 2000-2019, from monthly, seasonal, and annual mean OSTIA data. This is compared to the NWSPPE ensemble mean for the equivalent period. We also assess where the OSTIA 20-year mean sits within the NWSPPE (when processed equivalently), asking how many NWSPPE ensemble standard deviations OSTIA is form the NWSPPE ensemble mean.

2.2.2 EN4

We evaluate the surface and near bed temperature and salinity of the NWSPPE with the EN4 quality-controlled temperature and salinity profile dataset (Good et al., 2013). We use the individual observed vertical profiles of version EN.4.2.2.g10.

As the EN4 data are relatively sparse on the NWS, it is a complex data set to use in a climate context, and so we follow a similar methodology to Tinker et al. (2020). There are few EN4 locations where there are observations are available for every year for a given month and grid box, and so it is seldom possible to separate the observed climatology from the observed interannual variability. Therefore, rather than comparing the observed climatology from the distribution of NWSPPE climatologies (the distribution of the 20 year means from the NWSPPE), we compare the EN4 observation to the NWSPPE distribution of both interannual variability and ensemble variability (12 ensemble members and 20 years). This is a like-for-like analysis.

https://doi.org/10.5194/egusphere-2023-1816
Preprint. Discussion started: 18 August 2023

2.2.2.1 EN4 evaluation methodology

This comparison is designed to evaluate the broad characteristics of any model biases. A more detailed comparison is beyond the scope of the present study.

Creating the NWSPPE distribution fields.

1. We create a NWSPPE climatology.
    a. For each of the 12 months we average all the monthly means from all the ensembles between 2000 and 2019.
    b. As the EN4 data set is sparse, for each of the 12 months, we also calculate the ensemble standard deviation across all 240 points (20 years and 12 ensemble-members).

Pre-processing the EN4 data

2. We discard the profiles with QC flags ('POSITION_QC', 'PROFILE_POTM_QC', 'PROFILE_PSAL_QC') = 4.
3. For each month, and for each year, we:
    a. We assign each profile to the nearest COx grid box, and linearly interpolated it onto the vertical s-levels.
    b. If there are more than one profile for a given month, we average them.
    c. We calculate the normalised bias:

$$NormBias = \frac{\left(PPE\_mean_{i,j,z,m} - Obs_{i,j,z,y,m}\right)}{PPE\_std_{i,j,z,m}}$$

Where *i, j, z* are the grid index in three dimensions and *y* and *m* are the year and month.

    d. For each month, for each grid box we add all the NormBias from all the years, add the square of the NormBias, and count the number of years with an observation (Sum_NormBias, SSq_NormBias, cnt_NormBias).
    e. For each month, we can calculate the mean and the standard deviation of the NormBias for each grid box (Mean_NormBias, Std_NormBias).
    f. We can combine Sum_NormBias, SSq_NormBias, cnt_NormBias for each month into seasons (DJF, MAM, JJA, and SON), and annual means.

This gives us a gridded assessment, for each month, season, and year, of where the EN4 observations sit within the NWSPPE (SST: Figure S2; SSS: Figure S3; NBT: Figure S4). For each grid box with an EN4 observation, we can then give the number of NWSPPE standard deviation is it from the ensemble mean. If the grid box (for a given season or month), has observations from different years, they are averaged. These sparsely sampled maps are hard to use quantitatively, and so regional summaries are also produced (Figure 3).

2.2.3 Satellite SSH data

We evaluate the NWSPPE SSH following the methodology of Tinker et al. (2020), where we refer the reader for evaluation of PDCtrl SSH. We compare the mean pattern of the modelled sea level to satellite altimetry Mean Dynamic Topography (MDT), which indicates the average strength of the geostrophic currents (Hermans et al., 2020a). The pattern of the interannual SSH variability is compared to a satellite altimetry sea level anomaly product.

We use the AVISO MDT product (Figure 4c), estimated from the period 1993–2012 (Rio et al., 2014), and compare to the NWSPPE ensemble mean SSH for the present-day ensemble statistics (2000-2019). As AVISO has a lower horizontal resolution (0.25°), and is not able to resolve features with spatial wavelengths less than ~ 180 km (Legeais, 2018), we smooth model by convolving with a uniform filter of 13-by-13 grid boxes (~ 90 km, Figure 4a).

We compare the simulated interannual SSH variability is to that of the Copernicus Climate Change Service (C3S) Sea Level Anomaly (SLA) product (Legeais et al., 2018). We compute annual means (1993–2018) of the (daily, 0.25° horizontal resolution) C3S SLA product, linearly detrend (temporally), and calculate the temporal standard deviation. This is compared to the interannual variability from the present-day ensemble statistics (2000-2019) - the square root of σ^2_{int} from (1) in section 5.4.3.

https://doi.org/10.5194/egusphere-2023-1816
Preprint. Discussion started: 18 August 2023

2.2.4 Tide Gauge data

The NWSPPE was compared to 20 tide gauges around the UK and NWS (Figure 5), which were selected for the length of overlap with the NWSPPE. These were downloaded from the Permanent Service for Mean Sea Level (PSMSL, Holgate et al. (2013); Data retrieved 24th of November 2022), and processed into annual means. We use PSMSL monthly revised local reference (RLR) data to account for changing baselines and we reject data with quality issues (calculations for mean tide level, suspect data, etc.). Annual mean time-series are created from monthly mean anomalies (where the climatological season cycle has been removed) where there is data from at least 11 months.

The SSH from the nearest (sea) grid box was extracted from the monthly mean data, and processed into annual means, for each ensemble member and then processed into ensemble means. The tide gauges were not corrected for Glacial Isostatic Adjustment (GIA), and so Smögen (which exhibits substantial GIA) was excluded. For each tide gauge an offset between the ensemble mean was removed. This was the difference between the NWSPPE Ensemble mean temporal mean and tide gauge temporal mean, for the common overlap period.

https://doi.org/10.5194/egusphere-2023-1816
Preprint. Discussion started: 18 August 2023

3 Model and Methods

3.1 NEMO AMM7

We use the shelf seas version of NEMO (O'Dea et al., 2017) to dynamically downscale HadGEM3-GC3.05. It is run on the AMM7 NWS domain, which extends from 40° 4′ N 19° W to 65° N 13° E with a 7km horizontal resolution with hybrid terrain following vertical levels (s-levels, Siddorn and Furner (2013) for the PDCtrl and Bruciaferri et al. (2018) and Wise et al. (2022) for the transient projections).

Two slightly different version of the model are run for the Present-Day Control Simulation and the climate projections. Coastal Ocean version 6 (CO6), based on NEMO version 3.6, was used in the PDCtrl – see Tinker et al. (2020) for full details. Coastal Ocean version 9 (CO9, NEMO 4.04) is used for the NWSPPE climate projections. Tests showed little difference between the two models, so we consider the two versions to be consistent. We use COx when we refer to both model versions.

COx is driven by several different classes of boundary conditions. The atmospheric and ocean boundary conditions are provided by HadGEM3-GC3.05, and are interpolated onto the COx grid. The Baltic exchange and the rivers are specified by observation based climatologies. Full details of how these are implemented and their frequencies are given in Tinker et al. (2020) and their Table S9 in particular.

3.1.1 NEMO AMM7 tides

The standard version of NEMO introduces errors into the tides when using the 360-day climate. It resets the tides at the beginning of each month, and then runs sequentially. This leads to a jump at the end of the months with lengths other than 30 days. This doesn't seem to cause the model to crash but must affect the internal model solution. It also, on average, changes the M_2 period and so rendered standard tidal analysis useless.

We have adapted the tidal module within NEMO to work with the 360-day calendar, with three different methods: "reset", the standard method, where the tides are reset to every month; "drift" (which is used here), where we allow the tides to run continuously from a given date, but the annual tides (such as the equinoctial tides) drift by about 5 days every year, compared to the Gregorian calendar; and "compress", where we alter one of the astronomical frequencies within the tide module - this changes the M_2 (and most other) tidal frequency by ~2 seconds, but keeps the equinoctial tides with their correct timings. We describe these three methods and evaluate the impact they have on the tidal behaviour in appendix A. In these simulations, we use the drift method, where the model time, in number of seconds since 1st Jan 1980 (in the 360-day calendar), is counted forward with the Gregorian calendar to give the tidal conditions.

Both model versions use the same tidal constituents and tidal boundary conditions, however in the later version of NEMO (4.04) the default tidal Love Number was changed from 0.7 to 0, effectively turning off the internal tidal generating potential. This was not realised until the projections had been completed. In a small domain like the NWS, most tidal energy is propagated in from the boundary, and very little energy is internally generated, however this slightly affects the tidal range. A sensitivity test was run (running the unperturbed ensemble member with the tidal generating potential on and off) showing this only had a small impact on the tidal range (Figure S1), changing the amplitude of the M_2 tide by up to 4cm (which is up to about 3.5m). This was not considered significant for the climate projections, although in a different context (such as operational surge forecast systems), this could be more of a problem.

3.1.2 GitHub configurations.

Both NEMO configurations used in this study are available in GitHub.

NEMO version 3.6 CO6 (AMM7)

https://github.com/hadjt/NEMO_3.6_CO6_shelf_climate

Development of this configuration has frozen. The latest version available on GitHub was used in PDCtrl.

NEMO version 4.0.4 CO9 (AMM7 and AMM15)

https://doi.org/10.5194/egusphere-2023-1816
Preprint. Discussion started: 18 August 2023

https://github.com/hadjt/NEMO_4.0.4_CO9_shelf_climate/

Development of this configuration has continued since the NWSPPE was run.
The version used for NWSPPE is available as:
https://github.com/hadjt/NEMO_4.0.4_CO9_shelf_climate/tree/bddd0f68980632229c5afef9772c9fd0d0d6e930

A fix has since been added to set the default tidal Love Number to 0.7:
https://github.com/hadjt/NEMO_4.0.4_CO9_shelf_climate/tree/4ef0ec5e0c20a9aa88b42f395cc9b1bfd689a221

3.2 The HadGEM3-GC3.05 Perturbed Parameter Ensemble

HadGEM3-GC3.05 was run as a Perturbed Parameter Ensemble (PPE) for the UKCP18 climate projections. To explore the uncertainty associated with the choice of parameters and parameterisations within the GCM, a PPE perturbs the parameters (within a reasonable range) and chooses different parameterisations for each ensemble member. As more ensemble members are added, the sensitivity to these parameters increases the ensemble spread. This spread was designed to span the climate uncertainty associated with these uncertain parameters. The GCM simulations used, and the PPE framework are described in Sexton et al. (2021) and Yamazaki et al (2021).

Yamazaki et al (2021) ran a 25 member HadGEM3-GC3.05-PPE for the period 1900–2100, using CMIP5 historical and RCP8.5 emissions. The variants had different combinations of perturbations to 47 parameters in the model's atmosphere, land, and aerosol schemes, and they were selected by running a set of cheap, coarser-resolution atmosphere-only simulations from a large sample of nearly 3000 variants. Poor performing variants were filtered out by assessing retrospective 5-day weather forecasts and simulations of 2004–2009 with prescribed SST and sea ice. Further idealised atmosphere-only experiments were then used to select 25 variants which were as diverse as possible in terms of their atmospheric climate feedbacks and their regional responses to warmer SSTs (Sexton et al., 2021). These variants were then run with HadGEM-GC3.05 for historical and future simulations from 1900-2100 under RCP8.5. 10 members were dropped as being too cold by 1970, or when evaluated compared against 13 CMIP5 models over the historical period (1900-2005). The resulting 15 ensemble members gave plausible yet diverse atmosphere and ocean model behaviours (Yamazaki et al., 2021), and were used within the UKCP18 climate projections. Of this 15-member ensemble, 3 ensemble members exhibited unrealistic Atlantic Meridional Overturning Circulation (AMOC) behaviour and so were downscaled for the NWS, but were excluded from our analysis. The remaining 12 downscaled PPE is referred to as NWSPPE.

A heat and salinity flux adjustments as applied to the HadGEM3-GC3.05 PPE to prevent the surface climate from drifting too far from the realistic state despite the parameter perturbations giving rise to a range of net top-of-atmosphere radiative fluxes. Details of how the flux adjustments were applied are described in Yamazaki et al. (2021).

3.2.1 Present-Day Control Simulation

HadGEM3-GC3.05 was also run as a present-day control simulation for UKCP18, and underpinned Tinker et al. (2020). It was run for 270 years while simulating a stable climate equivalent to the year 2000. This was forced with green-house gases and aerosols from the year 2000 (as fixed values, or annually repeating seasonal cycles). This allowed the model to simulate the natural, unforced climate variability that would have occurred during the year 2000 and the absence of climate change. This simulation should capture the range of climate variability associated with different phases of climate modes such as El Nino Southern Oscillation, North Atlantic Oscillation, Atlantic Multidecadal Variability. The first 70 years of the simulation still show trends associated with the deep ocean spinning up, so the last 200 years were used for analysis by Tinker et al. (2020) and form the second part of this dataset. We refer to the downscaled control run as PDCtrl.

https://doi.org/10.5194/egusphere-2023-1816
Preprint. Discussion started: 18 August 2023

3.3 Copernicus Marine NWS Reanalysis (RAN)

A Met Office led consortia provided a marine reanalysis for the NWS to the Copernicus Marine Service (product number: NWSHELF_MULTIYEAR_PHY_004_009). This ran from 1993-2023 using the same regional shelf seas model and domain as used here (NEMO CO6). By running a shelf seas model, and assimilating observations (SST, temperature and salinity profiles, and satellite altimeters), it can be considered a best guess estimate of the current state of the NWS.

We make limited use of this NWS Reanalysis (hereinafter RAN), but comparing its regional mean time series (Tinker et al., 2019) to those of our NWSPPE. This gives some early-century context to the NWSPPE temporal evolution in terms of interannual variability and trends.

3.4 Experimental Design

We use CO9 to downscale the UKCP18 HadGEM3-GC3.05 PPE (Yamazaki et al., 2021). This ensemble is downscaled as transient simulations from January 1980-November 2099, but the first 10 years are considered spin up, and so are discarded. All 15 members of the PPE are downscaled, but three are excluded from this paper and associated data release. This leads to a 12 member PPE downscaled for the NWS (NWSPPE), from January 1990 to December 2098, for RCP8.5.

NWSPPE is consistent with PDCtrl, which can provide an estimate of a different source of uncertainty, and so the two datasets are released together.

3.5 Estimation of Time of Emergence (ToE)

We estimate the Time of Emergence (ToE) of the climate signal for SST and SSS, using the method of Lyu et al., (2014). We compare a modelled estimate of the present-day unforced variability (the noise, *N*), to the smoothed climate trend of an ensemble (the signal *S*) and ask when the ratio of the signal to noise is greater than a given threshold (2 standard deviations), doesn't drop below threshold for the rest of the record, and is at least 20 years long. We calculate the ToE for each ensemble member, and then report the median value, and the 16^{th}-84^{th} percentile range.

We estimate the Noise as the present-day unforced variability by taking the standard deviation of the linearly detrended PDCtrl annual means. As the PDCtrl has very little trend, detrending the PDCtrl has little effect on the ToE. We calculate the signal of each ensemble member by smoothing with a 4^{th} order polynomial and convert to anomalies by removing the 2000-2019 baseline-period. We then find where the *S*:*N* ratio exceeds the threshold, remains above the threshold for the rest of the simulation. We make one further criterion, that the ToE doesn't occur in the final 20 years of the projection (and so the emergence time is at least 20-year long), as they may not represent the true emergence of climate signals.

https://doi.org/10.5194/egusphere-2023-1816
Preprint. Discussion started: 18 August 2023

4 Evaluation

We evaluate the NWSPPE between 2000 and 2019 for tides, temperature, salinity, and sea surface height (Table 1). We show the modelled co-tidal charts and compare these to other modelling systems. We compare the modelled SST with the OSTIA analysis (Roberts-Jones et al., 2012), and temperature and salinity with the EN4 quality-controlled subsurface profiles dataset (Good et al., 2013). We compare the modelled sea surface height to tide gauge data retrieved from the Permanent Service for Mean Sea Level (PSMSL, Holgate et al. (2013) and two satellite products (Rio et al., 2014; Legeais et al., 2018).

Evaluating climate projections is always complicated by the fact that they are not designed to simulate the observed phase of weather and climate variability. For example, while the approximate number and frequency of warm years should agree with observations, their ordering will not. This means the climate must be evaluated, rather than the "weather". To do this, we compare the statistics of long records of observations with the models – we would expect a level of agreement between the 20-year mean (and standard deviation) of the model and the observations. This works well for SST, where there are satellite records since the 1990s, but other long time series of observations are relatively sparse. Another complication is that reality is a single realisation of what conditions could be expected, given the current state of the climate. If there were 100 worlds with today's greenhouse-gas and aerosol conditions, we would expect a range of temperatures, due to unforced variability – different states of the North Atlantic Oscillation, different states of the Atlantic Multidecadal Variability, different weather conditions. With our PPE, we have a range of realisations of the present-day climate, any of which could be the reality. We therefore ask if the observed climatology is consistent with the distribution of modelled climatologies (the NWSPPE). We do this by calculating the observed 20-year mean, and the modelled 20-year mean for each ensemble member. We then ask how many (PPE ensemble) standard deviations the observed 20-year mean is from the PPE ensemble mean. If the observations are within 2 standard deviations, we consider the PPE to be consistent with the observations.

The approach works well for SST, where there are monthly observations across the NWS every year between 2000-2019. It is complicated by the sparsity of the EN4 data, where there may only be a single observation for a given grid box for a 20-year period. This means the observed "weather" is not separated from the observed climate – this must be taken into consideration (see section 2.2.2.1).

4.1 Tidal evaluation

We have evaluated the tides by producing co-tidal charts for leading constituents. The tidal harmonic analysis is done online by CO9, for consecutive 20-year periods. We show the ensemble mean for the files created for the 2000-2019 period (Figure 1). The ensemble mean phase (angle) is converted to its northward and eastward component before averaging. The M_2 component visually agrees well with O'Dea et al. (2012, 2017).

4.2 Sea Surface Temperature

Figure 2 gives the absolute SST bias (NWSPPE ensemble mean minus OSTIA SST) for the 4 seasons. We also assess where OSTIA sits within the distribution of the NWSPPE – where the OSTIA SSTs are more than 2 standard deviations from the ensemble mean, we hatch out the biases in Figure 2.

We find that most of the NWS, over most of the year, the OSTIA SSTs are within NWSPPE, and less than 2 °C from the ensemble mean. The waters to the west of the UK tend to be warmer than OSTIA, particularly in the summer. The North Sea tends to be cooler than OSTIA, particularly in the spring and summer. Overall, we consider the NWSPPE to be consistent with the OSTIA analysis.

4.3 Sub-surface Temperature and Salinity

The EN4 data processing procedure (outlined in section 2.2.2.1) produces sparsely sampled maps of the NWS, at monthly, seasonal, or annual granularity. The seasonal maps are given in the supplement (SST: Figure S2; SSS: Figure S3; NBT: Figure S4), however as they are still relatively sparse, they are hard to interpret quantitatively. We have therefore averaged these data

https://doi.org/10.5194/egusphere-2023-1816
Preprint. Discussion started: 18 August 2023

across the evaluation regions (in green in e.g. Figure S2), and presented the regional means, and spread (2 time the spatial standard deviation) in Figure 3.

This shows that in most regions, and in most time so the year, the EN4 SST observations are within the PPE ensemble, although less so in the poorly sampled Norwegian Trench. The NBTs also tend to be within the PPE, and tends to agree with the SST in most regions and months. There is more disagreement with the EN4 SSS, with much greater spatial variability within the regions (reflecting the greater spatial variability in Figure S4). However, when averaging over the regions, the EN4 SSS is typically within the PPE ensemble.

4.4 Sea Surface Height

COx has a non-linear free surface, and so simulates the dynamic response of the sea level to the local dynamics of the model. This illuminates important aspects of the model behaviour. It is also a component of sea level but should not be used directly as a set of sea level projections (see section 5.5).

First, we compare the NWSPPE and the AVISO satellite MDT. There is a good agreement in the overall pattern, with a large-scale NW/SE gradient and a similar range of values. On the NWS, the highest levels are in the German Bight, with lower values in the northern North Sea, north of the Dooley Current.

We then compare the simulated interannual SSH variability is to that of the C3S SLA product (Legeais et al., 2018). There is good spatial agreement between the PPE and C3S SLA product. In the open ocean there is greater sea level variability in deeper regions (e.g. the Rockall trough and the Icelandic basin). On the shelf the greatest variability in both the PPE and the C3S SLA product is in the German Bight, and the lowest variability is in the Celtic Sea, and to the west of Ireland and adjacent the shelf break, this is more pronounced in the C3S SLA product.

There is good agreement in the trend and interannual variability of the tide gauges and the PPE. The interannual variability of the PPE Ensemble mean is averaged out, but the tide gauge variability tends to agree with the ensemble spread (ensemble mean ± 2 standard deviations). In most locations (apart from Dieppe and Bergen), there is a good agreement in the trends. The tide gauge at Dieppe was reinstalled in 2009, and the levels appear to have changed (https://psmsl.org/data/obtaining/stations/474.php), with the later values in closer agreement with nearby tide gauges (La Harve and Boulogne). The tide gauge at Bergen may be affected by GIA.

https://doi.org/10.5194/egusphere-2023-1816
Preprint. Discussion started: 18 August 2023

5 Dataset Description

The data underlying these NWSPPE projections, with the PDCtrl data, have been released on the CEDA website (https://catalogue.ceda.ac.uk/uuid/832677618370457f9e0a85da021c1312). Here we will describe these files, the data structure, and the available variables. For the NWSPPE we provide monthly means of two-dimensional variables for every ensemble member, month, and year between 1990 and 2098. We also provide climatological means and standard deviations for each ensemble member, for an early and late century period (2000-2019 and 2079-2098). We use these climatologies to provide ensemble statistics, which are the basis of many of our figures. We also provide regional mean time-series.

NEMO is discretised onto an Arakawa "C" grid, and so separates variables onto a T, U and V grid. Most scalar variables on the T grid (the centre of the grid boxes). The U and V grids are offset between the T points (at the edges of the grid boxes). Therefore, variables on the T grid have a different location (in terms of longitude and latitude) compared to their equivalent U and V grid. We use this distinction and have three sets of files, with most variables in the T grid files, and only the U and V components of the barotropic current in the U and V grid files. We expect the T grid files to be sufficient for most purposes and applications. We also calculate the barotropic current magnitude on the T grid (reported in the T grid files) – this gives users a first look at the circulation.

5.1 Directory structure

Here we describe the directory structure. At the highest level, the NWSPPE data (Tinker, 2023b) is separated from its resulting ensemble statistics (Tinker, 2023a), and the PDCtrl data(Tinker, 2023c). Under the NWSPPE data, there are sub-directories for each ensemble members, each of which have sub-directories for the annual files (`annual`), the regional mean files (`regmean`) and the climatologies (`clim`). PDCtrl has sub-directories for the annual files (`annual`) the regional mean files (`regmean`):

```
NWSClim

1) NWSPPE
   a) r001i1p00000
      i) annual
      ii)   regmean
      iii)  clim
      (repeated for all 12 NWSPPE ensemble members)
   b) …
2) EnsStats


3) PDCtrl
   a) annual
   b) regmean
```

5.2 File names

Here we give example file names to help explain our naming convention.

`NWSPPE/r001i1p00000/annual`

- `NWSClim_NWSPPE_r001i1p00000_1990_gridT.nc`
- `NWSClim_NWSPPE_r001i1p00000_1990_gridU.nc`
- `NWSClim_NWSPPE_r001i1p00000_1990_gridV.nc`

For the T, U and V grid files respectively, where the ensemble number and year change.

`NWSClim/NWSPPE/r001i1p00000/regmean`

- `NWSClim_NWSPPE_r001i1p00000_1990-2098_regmean.nc`

For the regional mean files. The regional mean files give monthly means for the whole period.

https://doi.org/10.5194/egusphere-2023-1816
Preprint. Discussion started: 18 August 2023

NWSClim/NWSPPE/r001i1p00000/clim

- NWSClim_NWSPPE_r001i1p00000_clim_xxx_YYYY-YYYY_gridT_mean.nc
- NWSClim_NWSPPE_r001i1p00000_clim_ xxx_YYYY-YYYY_gridT_stddev.nc

For the climatological mean and standard deviation respectively on the T grid – again the U and V grid variables are in separate files. The xxx denotes the monthly (m01-m12 for January to December), seasonal (djf (December to February), mam (March to May), jja (July to August), son (September to November) for winter, spring, summer or autumn respectively), or annual means (ann), and the YYYY-YYYY denotes the climatological period, and may be 2000-2019 or 2079-2098.

We note that the variable names are unchanged (SST in one file is the 20-year mean, and in the other the 20-year standard deviation). The long_name variable attribute is also unchanged, but the method is captured in the cell_method.

NWSClim/PDCtrl/annual

- NWSClim_PDCtrl_1990_gridT.nc
- NWSClim_PDCtrl_1990_gridU.nc
- NWSClim_PDCtrl_1990_gridV.nc

The PDCtrl monthly mean files are analogous to the NWSPPE files described above.

NWSClim/PDCtrl/regmean

- NWSClim_PDCtrl_2050-2250_regmean.nc

The NWSPPE regional mean files are analogous to the NWSPPE files described above.

NWSClim/EnsStats

- NWSClim_NWSPPE_EnsStats_clim_xxx_YYYYYYYY_gridT_stats.nc

For the ensemble statistics (on the T grid, U and V grid variables are in separate files), where xxx again denotes monthly, seasonal or annual means. While the ensemble statistics are produced for the same climatological period (i.e. YYYYYYYY can be 2000-2019 or 2079-2098), they are also produced for the difference between the periods, so YYYYYYYY can also be 2079-2098minus2000-2019.

Here the file contains 4 statistics per variable, and so the variable names are modified to give the statistic name – SST_ensmean, SST_ensvar, SST_intvar, SST_ensstd. The long name and cell methods also reflect the statistic.

5.3 Variables

The variables that we have released include sea surface (SS-), near bottom (NB-) Temperature (T) and Salinity (S), and their difference (DF-) (SST, NBT, DFT, SSS, NBS, DFS), Potential Energy Anomaly (PEA), Mixed Layer Depth (MLD) and Sea Surface Height (SSH), and the U and V components of the barotropic (depth mean) velocity (DMU and DMV), and barotropic (depth mean) speed (DMUV). These are all on the T grid, apart from DMU and DMV on the U and V grid respectively.

The regional mean time series include RegAveSST, RegAveNBT, RegAveDFT, RegAveSSS, RegAveNBS, RegAveDFS, RegAveSSH and RegAvePEA (the regional means of SST, NBT, DFT, SSS, NBS, DFS, SSH and PEA respectively) - all the T grid variables, apart from DMUV and MLD.

Additional variables and frequencies may be available to collaborators, contact the author for details.

https://doi.org/10.5194/egusphere-2023-1816
Preprint. Discussion started: 18 August 2023

5.4 File structure

Here we describe the monthly mean fields, climatologies and ensemble statistics available on the CEDA data centre.

The released dataset covers the period between 1990 and December 2098 and is in CF-compliant netCDF files (CF-convention 1.8).

5.4.1 Annual (two-dimensional fields)

Monthly mean data is available for all months from January 1990 to December 2098, for all 12 ensemble members, and the present-day control simulation from 2050-2250 (each year still representing the year 2000). For each year, there are three files for the model T, U and V grid, with 12 monthly means within each. All variables are on the T grid, apart from the U and V components of the barotropic velocity (on the U and V grid respectively). Only 2D data fields are being released, with 3D variables such as Temperature and Salinity being reduced to surface (SS-) and near-bed fields (NB-), and the difference between them (DF-).

Details of the files is given in Table 2, in terms of the netCDF variable names and their dimensions. The dimensions of the files are "time", "lon", "lat" and "bnds", (simplified to t, y, x and 2 respectively in Table 2). Time is given in seconds since 1950-01-01 00:00:00, using a 360_day calendar. The time variable (time) is supplemented by the time bounds (time _bounds), giving the start and end of the averaging period (hence having two dimensions). The data 2D data fields are references with the longitude (lon) and latitude (lat) variables in each of the files – these are slightly offset between the T, U and V grids, although this is unlikely to cause any difficulty in most applications. Time is given in as double-precision ("f8") floating point numbers, whereas other variables are given as single precision ("f4") floating point numbers.

5.4.2 Climatologies

The monthly mean files are used to produce 20-year early century (2000-2019) and late century (2079-2098) climatologies, giving the mean and standard deviation in separate files. These are produced for annual means (ann), seasonal means (djf, mam, jja, and son) as well as monthly means (m01-m12 for January to December). The netCDF files have the same format as outlined in Table 2. The time_bounds variable sets the start and end of the climatology. For climatologies with an even number of years, the average time can be misleading, especially for monthly or seasonal climatologies where, for example, a winter climatology time_counter will be for summer. However, if you think of 2 sequential summers, the average time (in seconds since 00:00 1/1/1950) will be the winter between them – this is an unfortunate, if correct, feature of climatologies with an even number of years.

5.4.3 Ensemble Statistics

These climatologies are used to produce the ensemble mean, ensemble variance and standard deviation and interannual variance. As the NWSPPE is designed to capture the likely uncertainty (spread) associated with uncertain parameter, rather than to give the most likely outcome, then ensemble mean is not the most likely value. However, the ensemble mean and the ensemble standard deviation, are a useful way to summarise the (typically Gaussian) distributions. While the ensemble standard deviation is simply the square root of the ensemble variance, we think it will be a more useful statistic, so we include it to save end users having to calculate it. We also give the interannual variability, following Tinker et al. (2016). These are given for the near-present day (2000-2019) and future period (2079-2098). For the difference between the periods (2079-2098minus2000-2019) the statistics are simply the difference between the future and present-day statistics. This is useful to show how the ensemble has changed (i.e. how the ensemble mean and ensemble standard deviation has changed), however, does not give information on the uncertainty associated with a projected change. We therefore provide two additional statistics in the ensemble statistics difference files, the projected ensemble mean (projensmean) and the projected ensemble standard deviations. Here, we remove the present-day climatological mean from the future climatological mean to give a resulting anomaly ensemble – we then calculate the ensemble mean and standard deviation. This is useful when we want to say how the SST has increased, with an estimate of the uncertainty on the projection, for example when we say the southern North Sea

https://doi.org/10.5194/egusphere-2023-1816
Preprint. Discussion started: 18 August 2023

winter SST increased by 3.55 °C (±1.20 °C), we are taking winter southern North Sea regional mean of SST_projensmean (3.55 °C) and (2x) SST_projensmean (1.20 °C).

We consider the late-century climate change by comparing the early-century (2000-2019) to the late-century (2079-2098), for monthly, seasonal, and annual means. These time slices have been updated since UKCP09 and the Minerva projections, partly to make them closer to the present, but also as the simulations started in 1980 rather than 1952.

Following Tinker et al. (2016) we use two times the standard deviation (2σ) to describe the ensemble spread (average ± x, where x = 2σ). We calculate 2σ for each grid box, for a given month (and season and year) across each of the 20-year time periods and plot these in Figure 6-Figure 9. The typical interannual variability, however, is often greater than the ensemble time mean spread. Tinker et al. (2016) developed a more sophisticated analysis of the ensemble variability by decomposing of the total variance (σ^2_{tot}) into an interannual variability component (σ^2_{int}), which is the mean of the 20-year interannual variances for each ensemble member, and an ensemble spread component (σ^2_{ens}), which is the variance of the 20-year means for the ensemble:

$$\sigma^2_{int} = \frac{\sum_{e,y}\left(\left(x_{e,y}\right)^2\right)}{n_e n_y} - \frac{\sum_e\left(\left(\frac{\sum_y x_{e,y}}{n_y}\right)^2\right)}{n_e} \quad (1)$$

$$\sigma^2_{ens} = \frac{\sum_e\left(\left(\frac{\sum_y x_{e,y}}{n_y}\right)^2\right)}{n_e} - \left(\frac{\sum_{e,y} x_{e,y}}{n_e n_y}\right)^2 \quad (2)$$

$$\sigma^2_{tot} = \sigma^2_{int} + \sigma^2_{ens} \quad (3)$$

$$= \frac{\sum_{e,y}\left(\left(x_{e,y}\right)^2\right)}{n_e n_y} - \frac{\sum_e\left(\left(\frac{\sum_y x_{e,y}}{n_y}\right)^2\right)}{n_e} + \frac{\sum_e\left(\left(\frac{\sum_y x_{e,y}}{n_y}\right)^2\right)}{n_e} - \left(\frac{\sum_{e,y} x_{e,y}}{n_e n_y}\right)^2$$

$$= \frac{\sum_{e,y}\left(\left(x_{e,y}\right)^2\right)}{n_e n_y} - \left(\frac{\sum_{e,y} x_{e,y}}{n_e n_y}\right)^2$$

where this decomposition uses the sum of squares formula and where $x_{e,y}$ denotes a variable (such as SST) for a given year y, and ensemble member e, n_y is the number of years in the sample (20) and n_e the number of ensemble members (12).

For each variable in the monthly means, there are now three ensemble statistics, so rather than produce three files, we have added a suffix to the variable name.

5.4.4 Regional Means

Maps of climatological means are good at showing spatial patterns and changes, but do not show how the system evolves temporally. Regional mean time series show how the system evolves, how the ensemble spread changes and also give an estimate of the NWS response to model parameter uncertainty. They also allow a first look at the data, to help inform a more detailed analysis. We follow the methodology of Tinker et al. (2019) by averaging the model fields over a relevant region mask every time step. We use the region mask of Wakelin et al. (2012) as it divides the NWS into regions that make geographic an oceanographic sense. We also include a "shelf" region, by combining several NWS regions (excluding the Atlantic, Norwegian Trench, Skagerrak/Kattegat and Armorican shelf regions) – when we refer to a NWS mean, or averaged over the NWS, we refer to this "shelf" region. NEMO calculates these regional means every time-step and then averages them into the monthly mean time series (hourly means are also available) which are released for SST, NBT, DFT, SSS, NBS, DFS, PEA, and SSH. We also include the Wakelin et al. (2012) region mask in the file (mask). The time, time_bounds, lat and lon (for the mask) variables are also in other files. The variables are prefixed by RegAve (e.g. RegAveSST, RegAveSSS, RegAvePEA), and have two dimensions – time and region. Two one-dimensional variables reg_id and cnt specific to region mean files are included reg_id and cnt. reg_id is the region id, and is a value from 0 to 13 – this aligns with the region names (given in the global attribute region_names). cnt is a count of the number of grid boxes within each region (ranging from 792-25523)

https://doi.org/10.5194/egusphere-2023-1816
Preprint. Discussion started: 18 August 2023

One difference in the regional means from NEMO 3.6 and NEMO 4.0.4 (used in PDCtrl and NWSPPE respectively) is that NEMO3.6 simply averaged the values of all the grid boxes in a region, while NEMO 4.0.4 takes an area weighted average. For a direct comparison between the two data sets, it is fairly easy to reprocess the regional means from the annual files, with or without area weighting. Example code is provided in the GitHub python package.

5.5 Sea Surface Height (SSH)

Care must be taken when using the projected SSH – this is not to be used directly as a sea level projection. Sea level is affected by a wide range of process, and so sea level projections are built up from several different models (Fox-Kemper et al., 2021). Furthermore, given the different resolutions between HadGEM3-GC3.05 and COx, the different sources of lateral boundaries for the Atlantic and Baltic, the absences of tides in the GCM, the SSH in COx is likely to diverge from HadGEM3-GC3.05. However, COx improves the representation of coastal ocean processes, and so does give additional information on sea level change (e.g. Hermans et al., 2020a, b; Tinker et al., 2020), but this is only part of the Sea Level puzzle (Palmer et al., 2018).

The SSH data provided here is obtained from downscaling the HadGEM3-GC3.05 simulation of ocean Dynamic Sea-Level (DSL). DSL is defined as the local height of the sea-surface above the geoid and is corrected to remove time-dependent variations of the sea-surface due to atmospheric loading referred to as the inverse barometer effect. In the driving model (HadGEM3-GC3.05) DSL is defined to have zero global ocean area mean, therefore in the downscaled simulations the SSH data is providing the local anomaly in geocentric sea-level that results from local ocean density (steric) and circulation (dynamic) effects. While COx does simulate tides and the inverse barometer effect, its representation of SSH change include only part of the drivers of sea-level change active in the real world, which we briefly outline below.

Sea level change arises from process that alter the total volume of water in the ocean column or processes that alter the mass of water by redistributing water mass between the oceans and the continental land-surface. Simulated changes to ocean density from climate models can be used to estimate the effect of changes in ocean volume. However, many important processes that alter ocean mass, notably the contributions from loss of land-ice mass are not included in climate models and estimates for these process must be supplied from offline models. Additionally, changes to distribution of water mass in the oceans and over the land surface will produce spatially varying patterns of sea-level change associated with the Earth's gravitational field, axial-rotation, and deformation of solid-earth surface. The effect of the Gravitation, Rotation and Deformation process referred to collectively as GRD must also be estimated using offline models. Finally local sea-level projections for a coastal location may refer to changes relative to a local solid surface rather (relative sea-level change) than a fixed geoid (geocentric sea-level change) and use additional models to account for local vertical movement of the land surface (e.g. subsidence). These disparate sources are pulled together into the Sea Level puzzle (Palmer et al., 2018).

5.6 Missing Data

Over the 110 years, 12 months and 12 ensemble members, there were 23 files that were not archived correctly. Most of these were recreated by averaging the daily mean files giving near identical files (with the difference at the noise level). 3 files (Table 3) could not be created this way, and so were replaced by averaging the monthly mean for the same month from the previous and following year. The approach should maintain the seasonal cycle, and any trends in the data, however, may impact some statistics, such as estimates of interannual variability. Full details of the replacement files are given in Table S1 and Table S2.

5.7 Calculation of the barotropic current speed on the T grid (DMUV)

The use of model currents can often be complicated, especially as the U and V grids are offset. Often maps of current speed are useful, as they give an illustration of circulation. We have therefore provided the barotropic current magnitude on the T grid. First, we interpolated the U and V components of the barotropic current on the T grid:

https://doi.org/10.5194/egusphere-2023-1816
Preprint. Discussion started: 18 August 2023

$$DMU\_T_{j,i} = \frac{\mathrm{DMU}_{j,(i-i)} + \mathrm{DMU}_{j,i}}{2} \quad (4)$$

$$DMV\_T_{j,i} = \frac{\mathrm{DMV}_{j,i} + \mathrm{DMV}_{(j-1),i}}{2}$$

Where DMU and DMU are the U and V components of the barotropic current on their native U and V grids, and once they have been converted onto the T-grid they become DMU_T and DMU_T respectively. We then calculated their magnitude (DMUV)

$$DMUV_{j,i} = \sqrt{\mathrm{DMU\_T}_{j,i}{}^2 + \mathrm{DMU\_T}_{j,i}{}^2} \quad (5)$$

5.8 Code

This post-processing was undertaken in python, and is available from GitHub as:
https://github.com/hadjt/NWS_simulations_postproc

5.9 Digital Object Identifier (DOI)

Each of the top-level datasets has been issued with a DOI.

Physical Marine Climate Projections for the North West European Shelf Seas: NWSPPE. 20 July 2023.
https://dx.doi.org/10.5285/edf66239c70c426e9e9f19da1ac8ba87

Physical Marine Climate Projections for the North West European Shelf Seas: PDCtrl. 20 July 2023.
https://dx.doi.org/10.5285/66e39885a60e4b6386752b1a295f268a

Physical Marine Climate Projections for the North West European Shelf Seas: EnsStats. 20 July 2023.
https://dx.doi.org/10.5285/bd375134bd8c4990a1e9eb6d199cc723

https://doi.org/10.5194/egusphere-2023-1816
Preprint. Discussion started: 18 August 2023

6 Results and Applications.

We now explore some of the results of the NWSPPE climate projections – we refer the reader to Tinker et al. (2020) for a description of the results of the present day control simulation. We first describe the spatial patterns of the climate projections, before turning to the temporal evolution with regional mean time series.

6.1 Present-Day and Projected Spatial Patterns

The NWS SST (Figure 6; Table 5) rises by 3.11 °C (±0.98 °C) by the end of the century, when averaged across the shelf (ensemble mean ± 2 ensemble standard deviations). There is a seasonal cycle in the warming, with greater warming in the summer (3.57 °C ±1.09 °C) and autumn (3.73 °C ±1.07 °C) than in the winter (2.72 °C ±0.97 °C) and spring (2.43 °C ±1.01 °C). This is consistent with the wider UKCP18 projections (Murphy et al., 2018) which exhibit greater warming in the summer than the winter, which increases the amplitude of the temperature seasonal cycle, and is consistent with their key findings of projected hotter drier summers, and warmer wetter winters (Lowe et al., 2019). There is a region of reduced warming to the NW of the NWS (e.g., 60°N 15°W) which is more visible in winter (it may be obscured by summer stratification) and may influence the NWS. A likely cause of this is the North Atlantic Warming Hole (Menary and Wood, 2018), and a reduction in the Atlantic Meridional Overturning Circulation (AMOC), transporting less heat from the tropical Atlantic. In the summer this may be masked by stratification. This will be considered later in the discussion.

On the NWS, the southern and central North Sea show considerable warming, particularly in summer and autumn, with typically greater than 3.5°C warming. The greatest NWS warming is in the Dover strait in autumn, where the ensemble mean SST warms by up to 5°C. There is an adjacent region of reduced warming in the centre of the Southern Bight (~52°N 3°E) in all seasons, relating to an apparent weakening of the warm plume of water flowing from the English Channel into the Southern North Sea (Figure S7).

The Near Bottom Temperatures exhibit a more modest rise than the SST (Figure 7), with an annual mean NWS NBT warming of 2.49 °C (±0.94 °C). This largely reflects a reduced warming under stratified regions. In the SST, we saw a greater warming in summer than winter. As the spring initialisation of stratification isolates bottom water from the atmosphere, NBTs remain close to the winter spring temperatures under stratification. Therefore, the weaker winter SST warming will reduce the summer NBT warming in stratified regions. This is illustrated in the difference in the southern and northern North Sea NBT summer warming, 3.55 °C (±1.00 °C) and 2.07 °C (±1.00 °C) respectively. The southern North Sea summer NBT rises to a similar level that of the SSTs in the same region and season (3.78 °C (±1.04 °C)), while the northern North Sea summer NBT warming is closer to the winter SSTs (2.71 °C (±0.99 °C)) than the summer SSTs (3.61 °C (±1.20 °C)) in the same region.

It is also interesting to note that the northern North Sea winter (and autumn) NBTs exhibit greater warming than the summer. The northern North Sea is the main place where the North Sea connects to North Atlantic, and so most affected by the reduced North Atlantic warming. In the winter, the northern North Sea may also be being warmed by the atmosphere, while when stratified, this would not be possible. This would tend to lead to a greater northern North Sea NBT rise in winter than in summer, as simulated.

There is a general strengthening in the magnitude of summer stratification, although there is little change in its extent. The strengthening is shown in the increase in Potential Energy Anomaly (PEA, Figure S5), and reflected by a substantial increase in the difference between SST and NBT (DFT) during stratified months (Figure 8).

There is a substantial freshening across the domain, which is greatest in the open ocean to the west of the domain. The NWS also shows substantial freshening, with -1.01 psu (±0.93 psu) when averaged over the shelf, and little spatial or seasonal variations. There is also substantial increase in the ensemble variance, and a much smaller increase in inter annual variability.

6.2 Regional Mean Timeseries

We have looked at the time mean spatial patterns of the NWSPPE. We now assess the regional means time series from the NWSPPE, to illuminate the NWS's temporal evolution. We also compare to the Copernicus Marine reanalysis (RAN) to

https://doi.org/10.5194/egusphere-2023-1816
Preprint. Discussion started: 18 August 2023

provide near present-day information for context (Figure 10, Figure 11). We note that our use of climatological Baltic boundary conditions may explain the behaviour and the reduced interannual variability in the Skagerrak/Kattegat and Norwegian Trench regions.

The SST regional mean time series are in relatively good agreement with the absolute values of the RAN reanalysis (Figure 10). There is a near linear trend in the ensemble mean SST. Each individual ensemble member also has near linear trends (typically $r > 0.9$), but have much larger interannual variability, which is averaged out in the ensemble mean (Figure S10). While the ensemble mean interannual variability appears much lower than that of RAN, there is relatively good agreement when comparing to individual ensemble members (Figure S10), particularly on the shelf. The RAN time series appear to have a different trend to the ensemble but is consistent with the scale of the variability of individual ensemble members (not shown). The SST ensemble spread remains relatively constant in some regions, and slightly widens in other regions. The SST interannual variability is also relatively constant throughout the projection (Figure S10). The annual mean NBT data show similar behaviour to that of the SST, so is not included in this paper.

The SSS regional mean time series tend to be saltier than the RAN reanalysis, which lies outside the ensemble spread in several regions. There is good agreement in interannual variability with the reanalysis in the North Sea and English Channel, while the PPE has greater interannual variability in other shelf regions. There is also a substantial increase in SSS interannual variability between 1990-2019 and 2069-2098 in almost all regions of the NWS (Figure S11) – absent in SST (Figure S10)

The NWS SSS behaves very differently to that of SST (Figure 10). Rather than near linear evolution seen in SST (Figure S8), SSS has an increasing freshening, and divergence of the ensemble. For most ensemble members, and shelf regions the correlation tends to improve when fitting different straight lines for the beginning and end parts if the time series (Figure S9).

7 Discussion

We have downscaled a PPE of HadGEM3-GC3.05 to give a set of climate projections for the NWS. The PPE was developed for the UKCP18 climate projections to explore the range of an important source of uncertainty in the climate projections and was run under the RCP8.5 scenario. We have downscaled 12 members of this PPE with the shelf seas model NEMO CO9 (NWSPPE) from 1990-2098 (plus a discarded 10-year spin up period). We have driven CO9 with atmospheric fluxes and ocean lateral boundary conditions interpolated directly from HadGEM3-GC3.05 (without any bias correction). We have used a climatology for the river forcings and for the exchange with the Baltic Sea.

We have undertaken extensive model evaluation (for SST, subsurface T and S, SSH and tides) and explored the first order change the NWS. These simulations represent the state-of-the-art for NWS marine projections.

This set of projections is closely related to, and compatible with, the 200-year present day control simulation of Tinker et al. (2020) (PDCtrl). We have combined both datasets into a single data release, which is also described here.

Our NWSPPE is a direct update to the Minerva Projections released in 2016. The same general approach is taken, downscaling the PPE run for UKCP, with a regional shelf seas model, to give a similar set of physical projections. Minerva downscaled the UKCP09 PPE which was based on HadCM3 (Gordon et al., 2000; Pope et al., 2000). HadCM3 was a relatively old model at the time (being a CMIP3 generation model) but was used as it is computationally efficiency allowed it to be run many times in the ensemble. We use the latest Met Office Hadley Centre CMIP6 generation model HadGEM3-GC3.05. Minerva was based on POLCOMS (Holt and James, 2001; Holt et al., 2001), a 12km resolution shelf seas model which had already been replaced at the Met Office in favour of NEMO Coastal Ocean model. Here we used NEMO version 4.04, an even more recent version than is used operationally at the Met Office. As the HadCM3 atmosphere has a horizonal resolution of 2.5° latitude by 3.75° longitude, a regional atmosphere climate model (HadRM3, ~25km horizontal resolution, Jones et al., 2004) was used to downscale the HadCM3 atmosphere to provide atmospheric forcings to POLCOMS. As the HadRM3 model domain didn't cover the full POLCOMS model, the southwest corner had to be cut off. HadGEM3-GC3.05 is of a much higher resolution (~60km) than HadCM3, and so the atmosphere did not need to be downscaled to produce the atmospheric forcing for NEMO.

https://doi.org/10.5194/egusphere-2023-1816
Preprint. Discussion started: 18 August 2023

Our projections are run under the RCP8.5 scenario, while the Minerva projections were based on the SRES A1B scenario (Nakicenovic et al., 2000). There is a greater warming in RCP8.5 compared to SRES A1B, with the UK region projected to warm by 3.9°C in 2080-2099 relative to 1981-2000 under RCP8.5 compared to 2.7°C under SRES A1B (Lowe et al., 2019) (the 50th percentile of the UKCP18 terrestrial probabilistic projections). Furthermore, all HadGEM3-GC3.05 PPE members have a relatively high climate sensitivity (Rostron et al., 2020), similar to HadGEM3-GC3.1 and greater than that of HadCM3 (Andrews et al., 2019), which was used in the Minerva projections. This greater warming is reflected in our new projections. We project an SST rise of 3.11 °C ($\pm 2\sigma$ = 0.98 °C), and an SSS freshening of −1.01 psu ($\pm 2\sigma$ = 0.93 psu) for 2079-2098 relative to 2000-2019. Tinker et al. (2016) projected shelf and annual mean SST rise of 2.90 °C ($\pm 2\sigma$ = 0.82 °C), and an SSS freshening of -0.41 psu ($\pm 2\sigma$ = 0.47 psu) for 2069–2098 relative to 1960–1989. It is difficult to directly compare these changes due to the changes in baseline however, we note that we project a greater change over a shorter period.

When we plot the regional mean time series for both sets of projection, as anomalies relative to a common baseline, the difference is more striking (Figure 12). While both Minerva and the NWSPPE show a near-linear SST rise and similar ensemble divergence, there is a notably greater rate of warming in our new projections. When looking at SSS, the difference is striking. While the Minerva projections showed a substantial reduction in salinity, we show a much greater freshening. In the Minerva projections, the ensemble mean salinity is mainly driven by a steplike change in a few ensemble members with particularly high climate sensitivity. Almost all our ensemble members show a substantial increase in the rate for freshening (Figure S9) driving a much greater ensemble mean change. Figure 9 suggests the salinity changes are driven by changes in the salinity in the open ocean adjacent the NWS.

Over most of the NWS, we show a similar pattern of SST change to Minerva (Tinker et al., 2016) with the southern North Sea showing the greatest warming, and the SST fingerprint of a reducing shelf break current to the north and west of Scotland (Figure 6). When we look across the whole model domain, we see important differences in the SST change spatial pattern (compared to Minerva). The most striking difference is the area of near zero winter (and spring) warming in the open ocean to the North West of the domain in NWSPPE, which is absent in Tinker et al. (2016). This is consistent with a slowdown in the AMOC and the associated North Atlantic warming hole (Drijfhout et al., 2012). Figure S12 (maps of the correlation between AMOC slow down and NWS change) show a concurrent region of highly correlated SSTs to the south of Iceland, and a pattern of highly correlated NBTs in the deep waters to the west of the NWS. These correlations reflect that the ensemble members with the weakest reduction in AMOC having the greatest warming locally, and also that the ensemble members with the strongest reduction in AMOC actually have local cooling. The tongue of highly correlated SSTs in the Icelandic Basin is a branch of the North Atlantic Current (Perez et al., 2018), while the pattern of the highly correlated NBTs reflect the complex deep water pathways and bathymetry of this region. There is a competition between the warming associated with a rising global mean temperature, and a cooling associate with a reduced AMOC (Drijfhout, 2015) - over most of the domain, the warming dominates, whereas in this small region, the cooling dominates, resulting in a region of negligible projected SST warming.

We also see a region of reduced warming in the Southern Bight (e.g. Figure 6). There is eastward transport bringing warm water from the English Channel into the Southern Bight of the North Sea, which leads to a plume of warmer, saltier water (e.g. Tinker et al. (2022). This eastward volume transport decreases into the future (Figure S7), as does the associated heat transport. This weakens the Southern Bight warm plume, so reduces the localised warming.

As our NWSPPE is consistent to the PDCrtl, the two data set can be used together. By using the projected climate evolution from NWSPPE, with the estimated unforced variability of the PDCtrl, it is possible, for example, to estimate the Time of Emergence of the climate signal from that climate variability. Most GCM climate projections are started from a convenient point within a climate spin-up simulation, when the modelled climate is stable (or its drift is acceptable), and time counter started from the year 1850 to reflect the start of the “historical” forcing period. They do not use data assimilation (or a similar process) to constrain the present-day climate to observed state of reality, as in seasonal or decadal forecasting systems (e.g.

https://doi.org/10.5194/egusphere-2023-1816
Preprint. Discussion started: 18 August 2023

MacLachlan et al., 2014; Hermanson et al., 2022). This means that the present day of the climate simulation doesn't match reality, in terms of the phase of the various climate modes and variability. This does not matter in the distant future (late century) where we can be confident that the climate change signal dominates over the possible range of present-day variability, but potentially limits the utility of climate projections in the near future due to the potentially confounding influence of internal variability (e.g. IPCC, 2021). By estimating the Time of the climate signal Emergence (ToE), you can provide a lower bound of how soon you can start using uninitialised climate projections.

We have applied the method of Lyu et al., (2014) (described in section 3.5) to give an estimate of the Time of Emergence of the SST and SSS climate signal from the present day variability (Figure S13), and show the ensemble median and 16^{th}-84^{th} percentile range, masking out points where climate emerges in less than 84% of the ensemble (10 of the 12 members).

We find the SST climate signal emerges from variability across the shelf with a relatively low (16^{th} - 84^{th}) range across the ensemble, whereas the SSS signal only emerges the climate variability for 42% of the NWS (with emergence in greater than 10 ensemble members). Furthermore, the SSS climate signal emerges later than SST, and with greater ensemble spread. To compare the ToE of NWS SST and SSS, we take the NWS means of the ToE median (and range) for the grid boxes ToE emerges, and we find that the SST typically emerges in 2034 (with an 8-year range) while SSS emerges in 2046 with a 33-year range. This gives confidence in near future projections for periods later than this.

UK policy makers are interested in warming levels, such as the projected conditions under a 2°C and 4°C world. These are a useful policy tool to describe the climatic conditions when the when global mean temperatures rise to either 2°C or 4°C above pre-industrial levels. Warming levels have been used in the recent IPCC 4^{th} assessment report (IPCC, 2021) and in the UK's third Climate Change Risk Assessment (CCRA; Betts et al., 2021), and have been calculated for the UKCP18 HadGEM3-GC3.05 PPE. Gohar et al. (2018) use a time shifting methodology (Herger et al., 2015; Schleussner et al., 2016) to derive a pair of UKCP18 based 2°C and 4°C products. They use the HadGEM3-GC3.05 PPE (among other simulations) to find the years where the global mean temperature crosses the 2°C and 4°C threshold relative to the preindustrial conditions (considered to be 1851-1900). As we use the same PPE, the same years can be used as the basis of 2°C and 4°C projections of the NWS, however, as our simulations do not include the preindustrial period, some care must be taken when trying to apply and interpret this methodology to the NWSPPE. Their table 2 shows the timing of a centred 20-mean passing 2°C and 4°C of global mean temperature rise since the preindustrial period for the anonymised models in their study (adapted in our Table 9). For example, their model 1 (our r001i1p00000) passes the 2°C threshold in 2030, and the 4°C threshold in 2063. While we can calculate the NWS conditions for r001i1p00000 in a 20-year period centred on 2030 (2021-2040), and can iterate through our ensemble, we cannot show how much the NWS has change since the pre-industrial period, as our simulations start in 1980. Therefore, any difference between the NWS and the global mean that have occurred since the pre-industrial period are not captured. This is a common problem for regional studies. One approach is to say how different the NWS would be from the early century, under 2°C and 4°C warming levels. For this, for each ensemble member, we can use the time-slices in Table 9 and subtract the 2000-2019 period, and then average across the ensemble. Another approach is to add the global warming between 1850-1899 and 2000-2019 as calculated from the HadCRUT5 dataset (Morice et al., 2012), which equal 0.987°C. As the NWSPPE does not begin in the pre-industrial period, the exact timings of the 2°C and 4°C warming levels will still remain uncertain, especially as the HadGEM3-GC3.05 PPE was not designed to span all sources of uncertainty. The exact methodology used to choose the period of the 2°C and 4°C warming levels may impact the averaging periods, but the methodology proposed here should give a first order estimate.

These climate projections are a one-way forced downscaling of a GCM (HadGEM3-GC3.05) using climatological Baltic exchange, and rivers. This approach is based on two main assumptions. Firstly, that the driving GCM can simulate the large-scale climate and how it changes, and secondly, the downscaling approach allows improved resolution and additional physical processes important to the shelf seas, without becoming inconsistent with the climate of GCM.

https://doi.org/10.5194/egusphere-2023-1816
Preprint. Discussion started: 18 August 2023

HadGEM3-GC3.05 has been extensively evaluated at the global and regional scale (Williams et al., 2018), and for the parameters relevant for the NWS (Tinker et al., 2020). Dynamically downscaling GCMs for shelf seas regions is a well-established approach (Gröger et al., 2013; Mathis and Pohlmann, 2014; Tinker et al., 2016; Holt et al., 2010; Olbert et al., 2012). We follow the methodology of Tinker et al., (2020) using NEMO COx on AMM7, a very well established model and domain. NEMO COx is used operationally at the Met Office for 6-day forecasts (Tonani et al., 2019; O'Dea et al., 2017), and in their Reanalysis (Renshaw et al., 2019), both of which are currently part of the Copernicus Marine Service. Furthermore, it has been used as a research model on a number of time scales (including seasonal predictions (Tinker and Hermanson, 2021), centennial climate projections (Hermans et al., 2020b) and for the present day unforced climate variability (Tinker et al., 2020)). The choice of domain is important for downscaling – too big, and the interior of the model will diverge from the climate of the parent model, and too small and the boundary conditions will dominate the interior of the model. Furthermore, the geography of the domain is important, in the case of the NWS shelf edge processes are complex and should be either excluded (e.g. Olbert et al., 2012), or be far enough from the LBCs to behave independently from them. As NEMO COx run on the AMM7 domain has been extensively used and evaluated, we are convinced that our approach is fit for our purposes, although we do note some limitations.

We use a climatology for the Baltic exchange, which is a common approach (e.g. Tinker et al., 2015; Holt et al., 2010). The exchange with the Baltic is complex and helps controls the dynamics of the Norwegian Trench, so while this is not thought to have an impact on the UK, or most of the NWS, it may have an impact "downstream" of the Skagerrak (along the coast of Norway). This approach could be improved upon. A consistent set of transient Baltic Sea climate projections could give a trend to the climatology, or even a set of transient boundary conditions. It may be possible to develop a Baltic Sea box model to simulate the exchange (e.g. Stigebrandt, 1987). The best approach would be to run both NWS and Baltic projections together. Care must be taken with the mean sea level of the Atlantic and Baltic LBCs, which can be inconsistent when taken from different models. We also use a river climatology – using the river output from the GCM may be a better option but would need assessment. The estimated variability of the Baltic outflow (668 km^3yr^{-1} ±32 km^3 yr^{-1} for the period 2002-2021, Boulahia et al., 2022) appears relatively small compared to that of the North Sea riverine inflow – this may suggest that improving the representation of the riverine climate response is a greater priority.

We use the HadGEM3-GC3.05 atmosphere directly. This has a spatial resolution of about 70km, which is relatively low. Future projections may benefit from higher resolution atmosphere, however, there may be little benefit in increasing the atmospheric resolution until you get to convection permitting resolutions (~2 km) (e.g. Vautard et al., 2013; Kotlarski et al., 2014). This could either come from the using a higher resolution GCM, output from a regional atmospheric climate model to downscale the atmosphere, or by moving to a regional coupled climate model. Furthermore, other studies bias correct the GCM model output before use (Mathis et al., 2013). This could be explored for uncoupled future studies.

We use a COx on the AMM7 domain, which has a 7 km horizontal resolution, with 50 terrain following vertical levels. AMM7 is an eddy permitting model, but as the internal Rossby radius is ~4km on the NWS (Holt and Proctor, 2008), a model resolution greater than this would allow the simulation of a much richer eddy field, and improved representation of shelf exchange processes. AMM15 is a 1.5 km resolution model covering a similar region to AMM7. AMM15 will replace the use of AMM7 for many purposes. AMM15 is eddy resolving and shows an improved representation of the mean state across the domain, compared to AMM7 (Graham et al., 2018). As well as having a higher resolution, it requires a smaller timestep, so is much more expensive to run computationally that AMM7. Currently both AMM7 and AMM15 are run operationally at the Met Office to provide operational 6-day forecasts: AMM15 is coupled to a wave model; while AMM7 is coupled to the expensive biogeochemistry model as AMM15 to currently too expensive to run with biogeochemistry. AMM15 may be too expensive to use as the basis of ensemble climate projections. However, it may be useful to run companion runs, so show how these higher resolution processes may influence the projections.

https://doi.org/10.5194/egusphere-2023-1816
Preprint. Discussion started: 18 August 2023

Many users are interested estuaries or the coastal zone. These are currently beyond the scope of either AMM7 or AMM15. CO6 has a minimum depth of 10 m (in PDCtrl), to ensure the model doesn't dry out and crash. This is not necessary in CO9 (NWSPPE) where the wetting and drying module allows for more realistic coastal bathymetry. We suggest locations within three grid boxes of the land are used with care, and that the impact of the model's omission of coastal processes is considered on a case-by-case basis.

Our methodology uses an uncoupled, one-way forcing approach. While the HadGEM3-GC3.05 is coupled, and so implicitly includes coupled processes in the COx model forcings, COx is uncoupled, and so cannot feed back to the atmosphere or wider ocean. Coupled atmosphere ocean processes can be very important in the tropics, and there is increasing attention to their importance in the NWS. For example, forecasting sea fog (Fallmann et al., 2019), ocean-waves coupling Lagrangian trajectories (Bruciaferri et al., 2021), and heat waves (Petch et al., 2020), can be improved by using a regional coupled model. The Met Office is developing a regional ocean-atmosphere waves coupled model (UKC4) using the NEMO COx AMM15 model and the 2.2 km variable resolution MOGREPS UK (Hagelin et al., 2017) with the RAL3.1 scientific options (Flack et al., 2022). This will eventually couple with a biogeochemistry model and river model, to allow forecasting of multi-hazard compound events such as coastal flooding and erosion. This model is very complex and expensive to run, with the atmosphere component being much more expensive to run than the (already expensive) AMM15 model. While exploratory climate simulations of future time slices and case-studies are possible, this is even less likely than AMM15 to be used as the basis of an ensemble of transient climate projections. However, its use with an ensemble of projections can help understand what processes are poorly represented, and how the projections may be over or under predict certain phenomena, when compared to (things like) UKCP18.

Our NWSPPE give a quantification of one source of climate uncertainty. By varying parameters within the atmosphere, land and aerosol components of HadGEM3-GC3.05, the range of the response of the NWS climate can be assessed. This is an important source, but there are many other sources of uncertainty in climate projections. Other important sources include emission uncertainty, model structure uncertainty (of the global model, the shelf seas model, and even the regional atmospheric climate model), initial condition uncertainty, and methodological uncertainty (coupling and driving uncertainty). To date, the Minerva Projections (Tinker et al., 2016) have been the only systematic and comprehensive assessment of climate uncertainty within the NWS (Tinker and Howes, 2020). While our NWSPPE updates the Minerva Projections, they do not give any further insights in these other sources. A climate uncertainty budget for the NWS, which quantified and compared these sources, would be a useful contribution to the research field.

Our NWSPPE updates the Minerva Projections by making use of more advanced models, but does not extend their use. The next generation of NWS climate projections may couple to other components, such as a wave and or a biogeochemistry models – both of which are coupled to COx for the Met Office operational synoptic forecasts. This will represent the third (next) generation set of NWS climate projections.

Our approach updates the Minerva NWS climate projections, which were based on those of Holt et al. (2010). We feel that these projections are needed for the UK's upcoming 4th CCRA, but that the next set of UK climate projection should include the third generation NWS climate projections. These could address many of the limitations outlined above, by utilising: improved resolution (AMM15); improved coupling methodology (UKC4); additional model systems (biogeochemistry, waves/surge); different sources of uncertainty. These may require a range of methodologies, perhaps employing a cascade of model resolutions: AMM7 transient ensembles to address different sources of uncertainty, transient simulation of the standard ensemble member with AMM15, and case studies and times slices with UKC4. While coupling to a wave model does not increase the computational expense much (~10%), adding biogeochemistry does (3-6 times), so BGC may be limited to the lower resolution AMM7 (or with mixed resolution) simulations (as it is currently in operational forecasts). Adding biogeochemistry would allow a much wider range of end users to use the projections, while adding waves and surge would increase consistency and improve confidence. The next set of NWS climate projections may require a more community led

https://doi.org/10.5194/egusphere-2023-1816
Preprint. Discussion started: 18 August 2023

approach to support their greater complexity. Close proactive engagement and collaboration with end users during the planning and development stage will enable uptake, and the generation of user-relevant impacts to inform evidence-based coastal decision-making (Weeks et al., 2023).

805

https://doi.org/10.5194/egusphere-2023-1816
Preprint. Discussion started: 18 August 2023

8 Conclusions

Our key findings and conclusions are:

- The NWS annual mean SST rises by 3.11 °C (±0.98 °C) for 2079-2098 relative to 2000-2019, and with a greater warming in the summer and autumn.
- There is a region of limited warming in the deep water south of Iceland, associated with the AMOC slow down.
- There is substantial freshening across the NWS and domain, with the NWS freshening of −1.01 psu ($\pm 2\sigma$ = 0.93 psu) for 2079-2098 relative to 2000-2019. The rate of freshening increases through the 21st century.
- Using the NWSPPE with the PDCtrl allows the climate signal to be considered in the context of unforced natural variability. We give an example of how these can be used together to estimate the Time of Emergence of the climate signal emerges from the natural variability. For example, the ToE for the annual mean SST averaged over the NWS is 2025, suggesting that the entire ensemble has moved out of the natural variability compared to 2000-2019.
- The ToE gives confidence in the use of our projections in the mid-century, and we discuss how they could be used to simulate changes consistent with 2°C and 4 °C warming levels.
- These projections are for the physical environment, and so give no information about possible changes to the ecosystem (e.g. productivity, biomass, chlorophyll), biogeochemistry (e.g. nutrient levels, oxygen levels) or the wave conditions (e.g. significant wave height, wave period). In addition to including these other parameters, future marine climate projections may have greater spatial resolution, employ more sophisticated coupling strategies, and assess additional sources of climate projection uncertainty.

https://doi.org/10.5194/egusphere-2023-1816
Preprint. Discussion started: 18 August 2023

9 Code/Data Availability

The NWSPPE and PDCtrl datasets are available via CEDA (https://catalogue.ceda.ac.uk/uuid/832677618370457f9e0a85da021c1312), and can be accessed via their Digital Object Identifiers:

- https://dx.doi.org/10.5285/edf66239c70c426e9e9f19da1ac8ba87
- https://dx.doi.org/10.5285/66e39885a60e4b6386752b1a295f268a
- https://dx.doi.org/10.5285/bd375134bd8c4990a1e9eb6d199cc723

See section 5 (specifically section 5.9) for more information.

The post processing code (for the data release) is available on GitHub, see section 5.8 for more information.

The NEMO shelf climate configurations are also available on GitHub, see section 3.1.2 for more information.

10 Author Contribution

DS, KY and JR developed and ran the HadGEM3-GC3.05 PPE and added the specific diagnostics for the shelf seas downscaling. JT and MP designed the experiment. JT and EO adapted the NEMO configuration for use in the climate simulations. JT pre- and post-processed the files, undertook the analysis and visualisation of the data, and prepared the data release. BH helped with code review. JT, with MP and BH, prepared the initial manuscript, and all authors contributed to subsequent iterations.

11 Competing Interests

The authors declare that they have no conflict of interest.

12 Acknowledgement

All authors were supported by the Met Office Hadley Centre Climate Programme funded by BEIS and Defra.

We would like to thank several people who helped and advised during this study. Alex Arnold and Ségolène Berthou described the regional coupled configuration (UKC4). Carol McSweeney and Dan Bernie advised on the 2 °C and 4 °C warming levels. Daley Calvert helped move the NEMO configurations from the Met Office repository to GitHub. Leon Hermanson advised on the analysis and interpretation of the Atlantic Meridional Overturning Circulation (AMOC) slow-down. Richard Renshaw advised on the Copernicus Marine Reanalysis, and the Baltic Exchange. Fai Fung helped with the definition of the data set, and (with Carol McSweeney), the alignment with the UKCP18 project and datasets. Jeff Polton gave insight into the 360-day tides. Richard Renshaw helped with code review. We would particularly like to thank Diane Knappett and Ag Stephens for archiving and publishing the dataset.

https://doi.org/10.5194/egusphere-2023-1816
Preprint. Discussion started: 18 August 2023

13 References

Andrews, T., Andrews, M. B., Bodas-Salcedo, A., Jones, G. S., Kuhlbrodt, T., Manners, J., Menary, M. B., Ridley, J., Ringer, M. A., Sellar, A. A., Senior, C. A., and Tang, Y.: Forcings, Feedbacks, and Climate Sensitivity in HadGEM3-GC3.1 and UKESM1, J. Adv. Model. Earth Syst., https://doi.org/10.1029/2019MS001866, 2019.

Betts, R. A., Haward, A. B., and Pearson, K. V.: UK Climate Change Risk Assessment (CCRA3) Technical Report, London, 1478 pp., 2021.

Boulahia, A. K., García-García, D., Vigo, M. I., Trottini, M., and Sayol, J. M.: The Water Cycle of the Baltic Sea Region From GRACE/GRACE-FO Missions and ERA5 Data, Front. Earth Sci., https://doi.org/10.3389/feart.2022.879148, 2022.

Bruciaferri, D., Shapiro, G. I., and Wobus, F.: A multi-envelope vertical coordinate system for numerical ocean modelling, Ocean Dyn., https://doi.org/10.1007/s10236-018-1189-x, 2018.

Bruciaferri, D., Tonani, M., Lewis, H. W., Siddorn, J. R., Saulter, A., Castillo Sanchez, J. M., Valiente, N. G., Conley, D., Sykes, P., Ascione, I., and McConnell, N.: The Impact of Ocean-Wave Coupling on the Upper Ocean Circulation During Storm Events, J. Geophys. Res. Ocean., https://doi.org/10.1029/2021JC017343, 2021.

Drijfhout, S.: Competition between global warming and an abrupt collapse of the AMOC in Earth's energy imbalance, Sci. Rep., https://doi.org/10.1038/srep14877, 2015.

Drijfhout, S., van Oldenborgh, G. J., and Cimatoribus, A.: Is a decline of AMOC causing the warming hole above the North Atlantic in observed and modeled warming patterns?, J. Clim., https://doi.org/10.1175/JCLI-D-12-00490.1, 2012.

Eyring, V., Bony, S., Meehl, G. A., Senior, C. A., Stevens, B., Stouffer, R. J., and Taylor, K. E.: Overview of the Coupled Model Intercomparison Project Phase 6 (CMIP6) experimental design and organization, Geosci. Model Dev., https://doi.org/10.5194/gmd-9-1937-2016, 2016.

Fallmann, J., Lewis, H., Sanchez, J. C., and Lock, A.: Impact of high-resolution ocean–atmosphere coupling on fog formation over the North Sea, Q. J. R. Meteorol. Soc., https://doi.org/10.1002/qj.3488, 2019.

Flack, D. L. A., Bush, M., and Bohnenstengel, S.: Regional Atmosphere Land Configuration (RAL3): Assessment report, Exeter, EX1 3PB, UK, 90 pp., 2022.

Fox-Kemper, B., Hewitt, H., Xiao, C., Aðalgeirsdóttir, G., Drijfhout, S., Edwards, T., Golledge, N., Hemer, M., Kopp, R., Krinner, G., Mix, A., Notz, D., Nowiciki, S., Nurhati, I., Ruiz, J., Sallée, J., Slangen, A., and Yu, Y.: Ocean, Cryosphere and Sea Level Change, 2021.

Gohar, G., Bernie, D., Good, P., and Lowe, J. A.: UKCP18 Derived Projections of Future Climate over the UK, Met Off., 2018.

Good, S. A., Martin, M., and Rayner, N. A.: EN4: Quality controlled ocean temperature and salinity profiles and monthly objective analyses with uncertainty estimates, J. Geophys. Res. Ocean., 118, 6704–6716, https://doi.org/doi:10.1002/2013JC009067, 2013.

Gordon, C., Cooper, C., Senior, C. A., Banks, H., Gregory, J. M., Johns, T. C., Mitchell, J. F. B., and Wood, R. A.: The simulation of SST, sea ice extents and ocean heat transports in a version of the Hadley Centre coupled model without flux adjustments, Clim. Dyn., 16, 147–168, 2000.

Graham, J. A., O'Dea, E., Holt, J., Polton, J., Hewitt, H., Furner, R., Guihou, K., Brereton, A., Arnold, A., Wakelin, S., Castillo Sanchez, J. M., and Mayorga Adame, C. G.: AMM15: a new high-resolution NEMO configuration for operational simulation of the European north-west shelf, Geosci. Model Dev., 11, 681–696, https://doi.org/https://doi.org/10.5194/gmd-11-681-2018, 2018.

Gröger, M., Maier-Reimer, E., Mikolajewicz, U., Moll, A., and Sein, D.: NW European shelf under climate warming: implications for open ocean – shelf exchange, primary production, and carbon absorption, 10, 3767–3792, https://doi.org/doi:10.5194/bg-10-3767-2013, 2013.

Hagelin, S., Son, J., Swinbank, R., McCabe, A., Roberts, N., and Tennant, W.: The Met Office convective-scale ensemble,

https://doi.org/10.5194/egusphere-2023-1816
Preprint. Discussion started: 18 August 2023

MOGREPS-UK, Q. J. R. Meteorol. Soc., 143, 2846–2861, https://doi.org/10.1002/qj.3135, 2017.

Herger, N., Sanderson, B. M., and Knutti, R.: Improved pattern scaling approaches for the use in climate impact studies, Geophys. Res. Lett., https://doi.org/10.1002/2015GL063569, 2015.

Hermans, T. H. J., Le Bars, D., Katsman, C. A., Camargo, C. M. L., Gerkema, T., Calafat, F. M., Tinker, J., and Slangen, A. B. A.: Drivers of interannual sea-level variability on the Northwestern European Shelf in the satellite altimetry era, J. Geophys. Res., 2020a.

Hermans, T. H. J., Tinker, J., Palmer, M. D., Katsman, C. A., Vermeersen, B. L. A., and Slangen, A. B. A.: Improving sea-level projections on the Northwestern European shelf using dynamical downscaling, Clim. Dyn., 54, 1987–2011, https://doi.org/10.1007/s00382-019-05104-5, 2020b.

Hermanson, L., Smith, D., Seabrook, M., Bilbao, R., Doblas-Reyes, F., Tourigny, E., Lapin, V., Kharin, V. V., Merryfield, W. J., Sospedra-Alfonso, R., Athanasiadis, P., Nicoli, D., Gualdi, S., Dunstone, N., Eade, R., Scaife, A., Collier, M., O'Kane, T., Kitsios, V., Sandery, P., Pankatz, K., Früh, B., Pohlmann, H., Müller, W., Kataoka, T., Tatebe, H., Ishii, M., Imada, Y., Kruschke, T., Koenigk, T., Karami, M. P., Yang, S., Tian, T., Zhang, L., Delworth, T., Yang, X., Zeng, F., Wang, Y., Counillon, F., Keenlyside, N., Bethke, I., Lean, J., Luterbacher, J., Kolli, R. K., and Kumar, A.: WMO Global Annual to Decadal Climate Update A Prediction for 2021-25, Bull. Am. Meteorol. Soc., 103, E1117–E1129, https://doi.org/10.1175/BAMS-D-20-0311.1, 2022.

Holgate, S. J., Matthews, A., Woodworth, P. L., Rickards, Lesley, J., Tamisiea, Mark, E., Bradshaw, E., Foden, Peter, R., Gordon, K. M., Jevrejeva, S., and Jeff Pugh: New Data Systems and Products at the Permanent Service for Mean Sea Level, J. Coast. Res., 29, 493, https://doi.org/10.2112/JCOASTRES-D-12-00175.1, 2013.

Holt, J. and Proctor, R.: The seasonal circulation and volume transport on the northwest European continental shelf: A fine-resolution model study, J. Geophys. Res., 113, https://doi.org/C06021 10.1029/2006jc004034, 2008.

Holt, J., Wakelin, S., Lowe, J. A., and Tinker, J.: The potential impacts of climate change on the hydrography of the northwest European continental shelf, Prog. Oceanogr., 86, 361–379, https://doi.org/https://doi.org/10.1016/j.pocean.2010.05.003, 2010.

Holt, J. T. and James, I. D.: An s coordinate density evolving model of the northwest European continental shelf - 1, Model description and density structure, J. Geophys. Res., 106, 14015–14034, 2001.

Holt, J. T., James, I. D., and Jones, J. E.: An s coordinate density evolving model of the northwest European continental shelf 2, Seasonal currents and tides, J. Geophys. Res., 106, 14035–14053, 2001.

Howard, T., Palmer, M. D., and Bricheno, L. M.: Contributions to 21st century projections of extreme sea-level change around the UK, Environ. Res. Commun., https://doi.org/10.1088/2515-7620/ab42d7, 2019.

Hunke, E. C., Lipscomb, W. H., Turner, A. K., Jeffery, N., and Elliott, S. M.: CICE: The Los Alamos sea ice model, documentation and software, version 5.1 (Tech. Rep. LA-CC-06-012), Los Alamos National Laboratory, Los Alamos, NM, 2015.

IPCC: Summary for Policymakers (AR6), in: Climate Change 2021: The Physical Science Basis. Contribution of Working Group I to the Sixth Assessment Report of the Intergovernmental Panel on Climate Change, edited by: Masson-Delmotte, V., Zhai, P., Pirani, A., S.L.Connors, Péan, C., Berger, S., Caud, N., Chen, Y., Goldfarb, L., Gomis, M. I., Huang, M., Leitzell, K., Lonnoy, E., Matthews, J. B. R., Maycock, T. K., Waterfield, T., Yelekçi, O., Yu, R., and Zho, B., Cambridge University Press, Cambridge, United Kingdom and New York, NY, USA, 3−32, https://doi.org/doi:10.1017/9781009157896.001, 2021.

Jones, R. G., Noguer, M., Hassell, D. C., Hudson, D., Wilson, S. S., Jenkins, G. J., and Mitchell, J. F. B.: Generating High Resolution Climate Change Scenarios Using PRECIS, Met Office Hadley Centre, Exeter, UK., 2004.

Kotlarski, S., Keuler, K., Christensen, O. B., Colette, A., Déqué, M., Gobiet, A., Goergen, K., Jacob, D., Lüthi, D., Van Meijgaard, E., Nikulin, G., Schär, C., Teichmann, C., Vautard, R., Warrach-Sagi, K., and Wulfmeyer, V.: Regional climate modeling on European scales: A joint standard evaluation of the EURO-CORDEX RCM ensemble, Geosci. Model Dev., https://doi.org/10.5194/gmd-7-1297-2014, 2014.

https://doi.org/10.5194/egusphere-2023-1816
Preprint. Discussion started: 18 August 2023

Legeais, J.-F.: Quality Information Document for Copernicus Climate Change Service DUACS Products: SEALEVEL_*_PHY_CLIMATE_L4_REP_OBSERVATIONS_008_0*CLS, Toulouse, 8 pp., 2018.

Legeais, J. F., Ablain, M., Zawadzki, L., Zuo, H., Johannessen, J. A., Scharffenberg, M. G., Fenoglio-Marc, L., Joana Fernandes, M., Baltazar Andersen, O., Rudenko, S., Cipollini, P., Quartly, G. D., Passaro, M., Cazenave, A., and Benveniste, J.: An improved and homogeneous altimeter sea level record from the ESA Climate Change Initiative, Earth Syst. Sci. Data, https://doi.org/10.5194/essd-10-281-2018, 2018.

Lowe, J., Howard, T., Pardaens, A., Tinker, J., Holt, J., Wakelin, S., Milne, G., Leake, J., Wolf, J., Horsburgh, K., Reeder, T., Jenkins, G., Ridley, J., Dye, S., and Bradley, S.: UKCP09 Marine and coastal projections, Exeter, 99 pp., 2009.

Lowe, J. A., Bernie, D., Bett, P., Bricheno, L., Brown, S., Calvert, D., Clark, R., Eagle, K., Edwards, T., Fosser, G., Fung, F., Gohar, L., Good, P., Gregory, J., Harris, G., Howard, T., Kaye, N., Kendon, E., Krijnen, J., Maisey, P., McDonald, R., McInnes, R., McSweeney, C., Mitchell, J. F., Murphy, J., Palmer, M., Roberts, C., Rostron, J., Sexton, D., Thornton, H., Tinker, J., Tucker, S., Yamazaki, K., and Belcher, S.: UKCP18 Science Overview Report version 2.0, Met Off., 2019.

Lyu, K., Zhang, X., Church, J. A., Slangen, A. B. A., and Hu, J.: Time of emergence for regional sea-level change, Nat. Clim. Chang., 4, 1006–1010, https://doi.org/10.1038/nclimate2397, 2014.

MacLachlan, C., Arribas, A., Peterson, K. A., Maidens, A., Fereday, D., Scaife, A. A., Gordon, M., Vellinga, M., Williams, A., Comer, R. E., Camp, J., Xavier, P., and Madec, G.: Global Seasonal forecast system version 5 (GloSea5): a high-resolution seasonal forecast system, Q. J. R. Meteorol. Soc., 141, 1072–1084, https://doi.org/doi: 10.1002/qj.2396, 2014.

Mathis, M. and Pohlmann, H.: Projection of physical conditions in the North Sea for the 21st century, Clim. Res., 61, 1–17, https://doi.org/doi:10.3354/cr01232, 2014.

Mathis, M., Mayer, B., and Pohlmann, T.: An uncoupled dynamical downscaling for the North Sea: Method and evaluation, Ocean Model., 72, 153–166, https://doi.org/https://doi.org/10.1016/j.ocemod.2013.09.004, 2013.

Menary, M. B. and Wood, R.: An anatomy of the projected North Atlantic warming hole in CMIP5 models, Clim. Dyn., 50, 3063–3080, https://doi.org/https://doi.org/10.1007/s00382-017-3793-8, 2018.

Morice, C. P., Kennedy, J. J., Rayner, N. A., and Jones, P. D.: Quantifying uncertainties in global and regional temperature change using an ensemble of observational estimates: The HadCRUT4 data set, J. Geophys. Res. Atmos., https://doi.org/10.1029/2011JD017187, 2012.

Murphy, J. M., Harris, G. R., Sexton, D. M. H., Kendon, E. J., Bett, P. E., Clark, R. T., Eagle, K. E., Fosser, G., Fung, F., Lowe, J. A., McDonald, R. E., McInnes, R. N., McSweeney, C. F., Mitchell, J. F. B., Rostron, J. W., Thornton, H. E., Tucker, S., and Yamazaki, K.: UKCP18 Land Projections: Science Report, Met Off. Hadley Cent., 2018.

Nakicenovic, N., Alcamo, J., Davis, G., de Vries, B., Fenhann, J., Gaffin, S., Gregory, K., Grubler, A., Jung, T., Kram, T., La Rovere, E., Michaelis, L., Mori, S., Morita, T., Pepper, W., Pitcher, H. M., Price, L., Riahi, K., Roehrl, A., Rogner, H.-H., Sankovski, A., Schlesinger, M., Shukla, P., Smith, S. J., Swart, R., van Rooijen, S., Victor, N., Dadi, Z., and Press, C. U.: Special Report on Emissions Scenarios: A special report of Working Group III of the Intergovernmental Panel on Climate Change, IPCC, 2000.

O'Dea, E., Arnold, A. K., Edwards, K. P., Furner, R., Hyder, P., Martin, M. J., Siddorn, J., Storkey, D., While, J., Holt, J., and Lui, H.: An operational ocean forecast system incorporating NEMO and SST data assimilation for the tidally driven European North-West shelf, J. Oper. Oceanogr., 5, 3–17, https://doi.org/http://dx.doi.org/10.1080/1755876X.2012.11020128, 2012.

O'Dea, E., Furner, R., Wakelin, S., Siddorn, J., While, J., Sykes, P., King, R., Holt, J., and Hewitt, H.: The CO5 configuration of the 7 km Atlantic Margin Model: large-scale biases and sensitivity to forcing, physics options and vertical resolution, Geosci. Model Dev., 10, 2947–2969, https://doi.org/https://doi.org/10.5194/gmd-10-2947-2017, 2017.

Olbert, A. I., Dabrowski, T., Nash, S., and Hartnett, M.: Regional modelling of the 21st century climate changes in the Irish Sea, Cont. Shelf Res., 41, 48–60, https://doi.org/10.1016/j.csr.2012.04.003, 2012.

Palmer, M. D., Howard, T. P., Tinker, J., Lowe, J., Bricheno, L., Calvert, D., Edwards, T., Gregory, J. M., Harris, G., Krijnen,

https://doi.org/10.5194/egusphere-2023-1816
Preprint. Discussion started: 18 August 2023

J., Roberts, C. D., and Wolf, J.: UKCP18 Marine Report, Met Office Hadley Centre, Exeter, UK., 133 pp., 2018.

Palmer, M. D., Gregory, J. M., Bagge, M., Calvert, D., Hagedoorn, J. M., Howard, T., Klemann, V., Lowe, J. A., Roberts, C. D., Slangen, A. B. A., and Spada, G.: Exploring the Drivers of Global and Local Sea-Level Change Over the 21st Century and Beyond, Earth's Futur., https://doi.org/10.1029/2019EF001413, 2020.

Perez, F. F., Fontela, M., García-Ibáñez, M. I., Mercier, H., Velo, A., Lherminier, P., Zunino, P., De La Paz, M., Alonso-Pérez, F., Guallart, E. F., and Padin, X. A.: Meridional overturning circulation conveys fast acidification to the deep Atlantic Ocean, Nature, https://doi.org/10.1038/nature25493, 2018.

Petch, J. C., Short, C. J., Best, M. J., McCarthy, M., Lewis, H. W., Vosper, S. B., and Weeks, M.: Sensitivity of the 2018 UK summer heatwave to local sea temperatures and soil moisture, Atmos. Sci. Lett., https://doi.org/10.1002/asl.948, 2020.

Pingree, R. D. and Griffiths, D. K.: Sand transport paths around the British Isles resulting from M 2 and M 4 tidal interactions, J. Mar. Biol. Assoc. United Kingdom, 59, 497–513, https://doi.org/10.1017/S0025315400042806, 1979.

Pope, V. D., Gallani, P. R., Rowntree, P. R., and Stratton, R. A.: The impact of new physical parametrizations in the Hadley Centre climate model: HadAM3, Clim. Dyn., 16, 123–146, https://doi.org/10.1007/s003820050009, 2000.

Pugh, D.: Tides, Surges and mean sea-level, John Wiley and Sons, Chichester, 1987.

Pugh, D.: Socio-economic indicators of marine-related activities in the UK economy, The Crown Estate, 68 pp., 2008.

Renshaw, R., Wakelin, S. L., Mahdon, R., O'Dea, E., and Tinker, J.: Copernicus Marine Environment Monitoring Service Quality Information Document North West European Shelf Production Centre NORTHWESTSHELF_REANALYSIS_PHYS_004_009., Exeter, 60 pp., 2019.

Ridley, J. K., Blockley, E. W., Keen, A. B., Rae, J. G. L., West, A. E., and Schroeder, D.: The sea ice model component of HadGEM3-GC3.1, Geosci. Model Dev., https://doi.org/10.5194/gmd-11-713-2018, 2018.

Rio, M.-H., Mulet, S., and Picot, N.: Beyond GOCE for the ocean circulation estimate: Synergetic use of altimetry, gravimetry, and in situ data provides new insight into geostrophic and Ekman currents, Geophys. Res. Lett., 41, 8918–8925, https://doi.org/doi:10.1002/2014GL061773, 2014.

Roberts-Jones, J., Fiedler, E., and Martin, M. J.: Daily, Global, High-Resolution SST and Sea Ice Reanalysis for 1985–2007 Using the OSTIA System, J. Clim., 25, 6215–6232, https://doi.org/doi: http://dx.doi.org/10.1175/JCLI-D-11-00648.1, 2012.

Rostron, J. W., Sexton, D. M. H., McSweeney, C. F., Yamazaki, K., Andrews, T., Furtado, K., Ringer, M. A., and Tsushima, Y.: The impact of performance filtering on climate feedbacks in a perturbed parameter ensemble, Clim. Dyn., https://doi.org/10.1007/s00382-020-05281-8, 2020.

Schleussner, C.-F., Lissner, T. K., Fischer, E. M., Wohland, J., Perrette, M., Golly, A., Rogelj, J., Childers, K., Schewe, J., Frieler, K., Mengel, M., Hare, W., and Schaeffer, M.: Differential climate impacts for policy-relevant limits to global warming: the case of 1.5°C and 2°C, Earth Syst. Dyn., 7, 327–351, https://doi.org/https://doi.org/10.5194/esd-7-327-2016, 2016.

Sexton, D. M. H., McSweeney, C. F., Rostron, J. W., Yamazaki, K., Booth, B. B. B., Murphy, J. M., Regayre, L., Johnson, J. S., and Karmalkar, A. V.: A perturbed parameter ensemble of HadGEM3-GC3.05 coupled model projections: part 1: selecting the parameter combinations, Clim. Dyn., https://doi.org/10.1007/s00382-021-05709-9, 2021.

Siddorn, J. R. R. and Furner, R.: An analytical stretching function that combines the best attributes of geopotential and terrain-following vertical coordinates, Ocean Model., 66, 1–13, https://doi.org/10.1016/j.ocemod.2013.02.001, 2013.

Simpson, J. H. and Bowers, D.: Models of stratification and frontal movement in shelf seas, Deep Sea Res. Part A. Oceanogr. Res. Pap., 28, 727–738, 1981.

Stigebrandt, A.: A Model for the Vertial Circulation of the Baltic Deep Water, J. Phys. Oceanogr., 17, 1772–1785, https://doi.org/10.1175/1520-0485(1987)017<1772:AMFTVC>2.0.CO;2, 1987.

Tinker, J.: Physical Marine Climate Projections for the North West European Shelf Seas: EnsStats, https://doi.org/doi:10.5285/bd375134bd8c4990a1e9eb6d199cc723, 2023a.

Tinker, J.: Physical Marine Climate Projections for the North West European Shelf Seas: NWSPPE,

https://doi.org/10.5194/egusphere-2023-1816
Preprint. Discussion started: 18 August 2023

https://doi.org/doi:10.5285/edf66239c70c426e9e9f19da1ac8ba87., 2023b.

Tinker, J.: sical Marine Climate Projections for the North West European Shelf Seas: PDCtrl, https://doi.org/doi:10.5285/66e39885a60e4b6386752b1a295f268a, 2023c.

Tinker, J. and Hermanson, L.: Towards winter seasonal predictability on the North West European Shelf Seas., Front. Mar. Sci., 8, 698997, https://doi.org/https://doi.org/10.3389/fmars.2021.698997, 2021.

Tinker, J. and Howes, E. L.: The impacts of climate change on temperature (air and sea), relevant to the coastal and marine environment around the UK, Lowestoft, 30 pp., https://doi.org/10.14465/2020.arc01.tem, 2020.

Tinker, J., Lowe, J., Holt, J., Pardaens, A., and Wiltshire, A.: Validation of an ensemble modelling system for climate projections for the northwest European shelf seas, Prog. Oceanogr., 138, 211–237, https://doi.org/10.1016/j.pocean.2015.07.002, 2015.

Tinker, J., Lowe, J., Pardaens, A., Holt, J., and Barciela, R.: Uncertainty in climate projections for the 21st century northwest European shelf seas, Prog. Oceanogr., 148, 56–73, https://doi.org/10.1016/j.pocean.2016.09.003, 2016.

Tinker, J., Krijnen, J., Wood, R., Barciela, R., and Dye, S. R.: What are the prospects for seasonal prediction of the marine environment of the North-west European Shelf?, Ocean Sci., 14, 887–909, https://doi.org/10.5194/os-14-887-2018, 2018.

Tinker, J., Renshaw, R., Barciela, R., and Wood, R.: Regional mean time series for the Northwest European Shelf seas. In: Copernicus Marine Service Ocean State Report, Issue 3, J. Oper. Oceanogr., 12, s26–s30, https://doi.org/https://doi.org/10.1080/1755876X.2019.1633075, 2019.

Tinker, J., Palmer, M. D., Copsey, D., Howard, T. P., Lowe, J., and Hermans, T. H. J.: Dynamical downscaling of unforced interannual sea-level variability in the North-West European shelf seas, Clim. Dyn., https://doi.org/DOI 10.1007/s00382-020-05378-0, 2020.

Tinker, J., Polton, J. A., Robins, P. E., Lewis, M. J., and O'Neill, C. K.: The influence of tides on the North West European shelf winter residual circulation, Front. Mar. Sci., 9, https://doi.org/10.3389/fmars.2022.847138, 2022.

Tonani, M., Pequignet, C., King, R., Sykes, P., McConnell, N., and Siddorn, J. R.: Copernicus Marine Environment Monitoring Service Quality Information Document North West European Shelf Production Centre NORTHWESTSHELF_ANALYSIS_FORECAST_PHYS_004_013, Exeter, 46 pp., 2019.

Vautard, R., Gobiet, A., Jacob, D., Belda, M., Colette, A., Déqué, M., Fernández, J., García-Díez, M., Goergen, K., Güttler, I., Halenka, T., Karacostas, T., Katragkou, E., Keuler, K., Kotlarski, S., Mayer, S., van Meijgaard, E., Nikulin, G., Patarčić, M., Scinocca, J., Sobolowski, S., Suklitsch, M., Teichmann, C., Warrach-Sagi, K., Wulfmeyer, V., and Yiou, P.: The simulation of European heat waves from an ensemble of regional climate models within the EURO-CORDEX project, Clim. Dyn., https://doi.org/10.1007/s00382-013-1714-z, 2013.

Wakelin, S. L., Holt, J. T., and Proctor, R.: The influence of initial conditions and open boundary conditions on shelf circulation in a 3D ocean-shelf model of the North East Atlantic, Ocean Dyn., 59, 67–81, https://doi.org/10.1007/s10236-008-0164-3, 2009.

Wakelin, S. L., Holt, J., Blackford, J., Allen, I., Butenschön, M., and Artioli, Y.: Modeling the carbon fluxes of the northwest European continental shelf: Validation and budgets, J. Geophys. Res. Ocean., 117, C05020, https://doi.org/DOI: 10.1029/2011JC007402, 2012.

Walters, D., Baran, A., Boutle, I., Brooks, M., Earnshaw, P., Edwards, J., Furtado, K., Hill, P., Lock, A., Manners, J., Morcrette, C., Mulcahy, J., Sanchez, C., Smith, C., Stratton, R., Tennant, W., Tomassini, L., Van Weverberg, K., Vosper, S., Willett, M., Browse, J., Bushell, A., Dalvi, M., Essery, R., Gedney, N., Hardiman, S., Johnson, B., Johnson, C., Jones, A., Mann, G., Milton, S., Rumbold, H., Sellar, A., Ujiie, M., Whitall, M., Williams, K., and Zerroukat, M.: The Met Office Unified Model Global Atmosphere 7.0/7.1 and JULES Global Land 7.0 configurations, Geosci. Model Dev., 12, 1909–1963, https://doi.org/https://doi.org/10.5194/gmd-12-1909-2019, 2019.

Weeks, J. H., Fung, F., Harrison, B. J., and Palmer, M. D.: The evolution of UK sea-level projections, Environ. Res. Commun.,

https://doi.org/10.5194/egusphere-2023-1816
Preprint. Discussion started: 18 August 2023

5, 032001, https://doi.org/DOI 10.1088/2515-7620/acc020, 2023.

Williams, K. D., Copsey, D., Blockley, E., Bodas-Salcedo, A., Calvert, D., Comer, R. E., Davis, P., Graham, T., Hewitt, H. T., Hill, R., Hyder, P., Ineson, S., Johns, T. C., Keen, A. B., Lee, R. W., Megann, A., Milton, S. F., Rae, J. G. L., Roberts, M. J., Scaife, A., Schiemann, R., Storkey, D., Thorpe, L., Watterson, I. G., Walters, D. N., West, A., Wood, R. A., Woollings, T., and Xavier, P. K.: The Met Office Global Coupled model 3.0 and 3.1 (GC3 & GC3.1) configurations, J. Adv. Model. Earth Syst., 10, 357–380, https://doi.org/https://doi.org/10.1002/2017MS001115, 2018.

Wise, A., Harle, J., Bruciaferri, D., O'Dea, E., and Polton, J.: The effect of vertical coordinates on the accuracy of a shelf sea model, Ocean Model., https://doi.org/10.1016/j.ocemod.2021.101935, 2022.

Yamazaki, K., Sexton, D. M. H., Rostron, J. W., McSweeney, C. F., Murphy, J. M., and Harris, G. R.: A perturbed parameter ensemble of HadGEM3-GC3.05 coupled model projections: part 2: global performance and future changes, Clim. Dyn., 56, 3437–3471, https://doi.org/10.1007/s00382-020-05608-5, 2021.

https://doi.org/10.5194/egusphere-2023-1816
Preprint. Discussion started: 18 August 2023

14 Tables

Table 1 Overview of NWSPPE evaluation

Variable	Dataset	Method
Tidal phase and amplitude	O'Dea et al. (2012, 2017)	Co-tidal charts compared to evaluated AMM7 cotidal charts of O'Dea et al. (2012, 2017)
SST	OSTIA analysis (Roberts-Jones et al., 2012)	Ensemble mean biases for the 4 seasons, and assessment of where OSTIA is within the NWSPPE distribution
Sub-surface temperature and salinity	EN4 quality-controlled subsurface profiles dataset (Good et al., 2013).	Methodology adapted from Tinker et al. and outlined in section 2.2.2.
Mean sea level	AVISO MDT (Rio et al., 2014)	1993–2012 and compare to the NWSPPE ensemble mean SSH for the present-day ensemble statistics (2000-2019).
Sea Level interannual variability	Satellite: C3S SLA product (Legeais et al., 2018) Tide gauges: Permanent Service for Mean Sea Level (PSMSL, Holgate et al. (2013)	

https://doi.org/10.5194/egusphere-2023-1816
Preprint. Discussion started: 18 August 2023

Table 2 Details of NetCDF files.

Grid and File	NC variable name	NC variable Long-name	Data precision	Dimensions
T	time	Time	double	t
T	time_bounds	Time bounds	double	t,2
T	lat	Latitude	float	y
T	lon	Longitude	float	x
T	SSH	Sea Surface Height above Geoid	float	t,y,x
T	SST	Sea Surface Temperature	float	t,y,x
T	SSS	Sea Surface Salinity	float	t,y,x
T	NBT	Near Bed Temperature	float	t,y,x
T	NBS	Near Bed Salinity	float	t,y,x
T	DFT	Difference between Sea Surface and Near Bed Temperature	float	t,y,x
T	DFS	Difference between Sea Surface and Near Bed Salinity	float	t,y,x
T	PEA	Potential Energy Anomaly	float	t,y,x
T	MLD	Mixed Layer Depth using Kara approach	float	t,y,x
T	DMUV	Barotropic current speed on T grid	float	t,y,x
U	time	Time	double	t
U	time_bounds	Time bounds	double	t,2
U	lat	Latitude	float	y
U	lon	Longitude	float	x
U	DMU	Eastward Ocean Barotropic current	float	t,y,x
V	time	Time	double	t
V	time_bounds	Time bounds	double	t,2
V	lat	Latitude	float	y
V	lon	Longitude	float	x
V	DMV	Northward Ocean Barotropic current	float	t,y,x

1090

https://doi.org/10.5194/egusphere-2023-1816
Preprint. Discussion started: 18 August 2023

Table 3 Files missing from the NWSPPE, that we recreated by averaging adjacent files.

Ensemble Member	Date	File type
r001i1p02242	205105	U grid Month Mean
r001i1p02868	205111	T grid Monthly Mean
r001i1p02832	205006	Regional mean time series

1095

https://doi.org/10.5194/egusphere-2023-1816
Preprint. Discussion started: 18 August 2023

Table 4 Tide gauges used for model comparison.

ID	Name	Longitude	Latitude	Period
01	Aberdeen I	-2.08	57.14	1931-2022
02	Bergen	5.32	60.40	1915-2022
03	Brest	-4.49	48.38	1807-2021
04	Cherbourg	-1.64	49.65	1974-2021
05	Delfzijl	6.93	53.33	1865-2022
06	Den Helder	4.75	52.96	1865-2022
07	Dieppe	1.08	49.93	1954-2021
08	Holyhead	-4.62	53.31	1938-2022
09	Immingham	-0.19	53.63	1959-2022
10	La Rochelle, La Pallice	-1.22	46.16	1941-2021
11	Lerwick	-1.14	60.15	1957-2022
12	Lowestoft	1.75	52.47	1955-2022
13	Newhaven	0.06	50.78	1991-2022
14	Newlyn	-5.54	50.10	1915-2022
15	North Shields	-1.44	55.01	1895-2022
16	Sheerness	0.74	51.45	1832-2022
17	St Nazaire	-2.20	47.27	1941-2021
18	Stornoway	-6.39	58.21	1977-2022
19	Tobermory	-6.06	56.62	1989-2022
20	Wick	-3.09	58.44	1965-2022

https://doi.org/10.5194/egusphere-2023-1816
Preprint. Discussion started: 18 August 2023

1100

Table 5 Projected regional mean SST changes between 2000-2019 and 2079-2098. Ensemble mean changes are given with ±2 (ensemble) standard deviations.

	Shelf	Southern North Sea	Central North Sea	Northern North Sea	English Channel	Irish Sea	Celtic Sea
ANN	3.11 °C (±0.98 °C)	3.72 °C (±1.03 °C)	3.59 °C (±1.07 °C)	3.14 °C (±1.02 °C)	3.34 °C (±0.88 °C)	3.22 °C (±1.03 °C)	3.01 °C (±0.90 °C)
DJF	2.72 °C (±0.97 °C)	3.55 °C (±1.20 °C)	3.20 °C (±1.07 °C)	2.71 °C (±0.99 °C)	3.06 °C (±0.95 °C)	3.03 °C (±1.00 °C)	2.43 °C (±0.83 °C)
MAM	2.43 °C (±1.01 °C)	3.02 °C (±1.08 °C)	2.97 °C (±1.16 °C)	2.56 °C (±1.08 °C)	2.69 °C (±0.88 °C)	2.56 °C (±1.04 °C)	2.21 °C (±0.87 °C)
JJA	3.57 °C (±1.09 °C)	3.78 °C (±1.04 °C)	4.05 °C (±1.18 °C)	3.61 °C (±1.20 °C)	3.71 °C (±0.91 °C)	3.67 °C (±1.09 °C)	3.62 °C (±0.96 °C)
SON	3.73 °C (±1.07 °C)	4.55 °C (±1.06 °C)	4.11 °C (±1.07 °C)	3.68 °C (±1.05 °C)	3.88 °C (±0.96 °C)	3.65 °C (±1.11 °C)	3.78 °C (±1.12 °C)

https://doi.org/10.5194/egusphere-2023-1816
Preprint. Discussion started: 18 August 2023

Table 6 Projected regional mean NBT changes between 2000-2019 and 2079-2098. See Table 5 for details.

	Shelf	Southern North Sea	Central North Sea	Northern North Sea	English Channel	Irish Sea	Celtic Sea
ANN	2.49 °C (±0.94 °C)	3.65 °C (±1.01 °C)	2.84 °C (±0.96 °C)	2.28 °C (±0.96 °C)	3.15 °C (±0.85 °C)	2.87 °C (±0.97 °C)	2.19 °C (±0.87 °C)
DJF	2.71 °C (±0.99 °C)	3.54 °C (±1.20 °C)	3.18 °C (±1.07 °C)	2.57 °C (±0.98 °C)	3.06 °C (±0.95 °C)	3.01 °C (±1.00 °C)	2.37 °C (±0.89 °C)
MAM	2.39 °C (±1.02 °C)	2.98 °C (±1.07 °C)	2.83 °C (±1.10 °C)	2.41 °C (±1.04 °C)	2.63 °C (±0.86 °C)	2.43 °C (±1.01 °C)	2.24 °C (±0.92 °C)
JJA	2.29 °C (±0.95 °C)	3.55 °C (±1.00 °C)	2.43 °C (±0.99 °C)	2.07 °C (±1.00 °C)	3.25 °C (±0.83 °C)	2.63 °C (±0.97 °C)	2.09 °C (±0.88 °C)
SON	2.58 °C (±0.94 °C)	4.53 °C (±1.06 °C)	2.90 °C (±0.89 °C)	2.06 °C (±0.97 °C)	3.66 °C (±0.93 °C)	3.42 °C (±1.04 °C)	2.08 °C (±0.87 °C)

https://doi.org/10.5194/egusphere-2023-1816
Preprint. Discussion started: 18 August 2023

Table 7 Projected regional mean DFT (SST – NBT) changes between 2000-2019 and 2079-2098. See Table 5 for details.

	Shelf	Southern North Sea	Central North Sea	Northern North Sea	English Channel	Irish Sea	Celtic Sea
ANN	0.62 °C (±0.34 °C)	0.07 °C (±0.04 °C)	0.75 °C (±0.36 °C)	0.86 °C (±0.44 °C)	0.19 °C (±0.08 °C)	0.35 °C (±0.14 °C)	0.82 °C (±0.41 °C)
DJF	0.01 °C (±0.16 °C)	0.01 °C (±0.02 °C)	0.02 °C (±0.03 °C)	0.14 °C (±0.16 °C)	0.00 °C (±0.01 °C)	0.02 °C (±0.03 °C)	0.06 °C (±0.24 °C)
MAM	0.03 °C (±0.27 °C)	0.04 °C (±0.04 °C)	0.14 °C (±0.22 °C)	0.15 °C (±0.25 °C)	0.06 °C (±0.05 °C)	0.13 °C (±0.10 °C)	-0.03 °C (±0.38 °C)
JJA	1.28 °C (±0.63 °C)	0.23 °C (±0.14 °C)	1.63 °C (±0.75 °C)	1.53 °C (±0.78 °C)	0.46 °C (±0.19 °C)	1.04 °C (±0.39 °C)	1.53 °C (±0.67 °C)
SON	1.15 °C (±0.60 °C)	0.02 °C (±0.02 °C)	1.20 °C (±0.63 °C)	1.62 °C (±0.89 °C)	0.22 °C (±0.12 °C)	0.23 °C (±0.15 °C)	1.70 °C (±0.70 °C)

https://doi.org/10.5194/egusphere-2023-1816
Preprint. Discussion started: 18 August 2023

Table 8 Projected regional mean SSS changes between 2000-2019 and 2079-2098. See Table 5 for details.

	Shelf	Southern North Sea	Central North Sea	Northern North Sea	English Channel	Irish Sea	Celtic Sea
ANN	-1.01 psu (±0.93 psu)	-0.94 psu (±1.00 psu)	-0.97 psu (±0.94 psu)	-1.06 psu (±1.03 psu)	-0.81 psu (±0.80 psu)	-0.98 psu (±0.77 psu)	-0.97 psu (±0.79 psu)
DJF	-1.01 psu (±0.92 psu)	-0.90 psu (±1.01 psu)	-0.96 psu (±0.92 psu)	-1.06 psu (±1.02 psu)	-0.80 psu (±0.79 psu)	-0.96 psu (±0.78 psu)	-0.98 psu (±0.79 psu)
MAM	-1.02 psu (±0.92 psu)	-0.94 psu (±1.01 psu)	-0.99 psu (±0.93 psu)	-1.08 psu (±1.02 psu)	-0.83 psu (±0.78 psu)	-1.02 psu (±0.78 psu)	-0.97 psu (±0.77 psu)
JJA	-1.00 psu (±0.94 psu)	-0.96 psu (±1.02 psu)	-0.97 psu (±0.96 psu)	-1.02 psu (±1.05 psu)	-0.81 psu (±0.82 psu)	-1.01 psu (±0.78 psu)	-0.94 psu (±0.79 psu)
SON	-1.02 psu (±0.95 psu)	-0.94 psu (±1.00 psu)	-0.95 psu (±0.96 psu)	-1.05 psu (±1.09 psu)	-0.80 psu (±0.82 psu)	-0.92 psu (±0.76 psu)	-0.97 psu (±0.83 psu)

https://doi.org/10.5194/egusphere-2023-1816
Preprint. Discussion started: 18 August 2023

Table 9 Timings of exceeding global mean warming levels of 2°C and 4 °C from the UKCP18 HadGEM3-GC3.05 PPE. The global warming levels are derived from the model simulated global annual mean anomaly relative to 1981-2000 baseline plus the observed warming from 1850-1900 mean to 1981-2000 mean based on HadCRUT4 (Morice et al., 2012) Timings are based on a centred 25 year running mean. While all simulations pass 2 °C of global mean warming some simulations to no reach global mean warming levels of 4 °C by the end of the century. Adapted from Gohar et al. (2018)

Ensemble Member	Global 2°C earliest passing, and range	Global 4°C earliest passing, and range
r001i1p00000	2030 (2021-2040)	2063 (2054-2073)
r001i1p00605	2027 (2018-2037)	2061 (2052-2071)
r001i1p00834	2030 (2021-2040)	2060 (2051-2070)
r001i1p01113	2027 (2018-2037)	2060 (2051-2070)
r001i1p01554	2032 (2023-2042)	2066 (2057-2076)
r001i1p01649	2029 (2020-2039)	2064 (2055-2074)
r001i1p01843	2031 (2022-2041)	2064 (2055-2074)
r001i1p01935	2032 (2023-2042)	2070 (2061-2080)
r001i1p02123	2028 (2019-2038)	2057 (2048-2067)
r001i1p02242	2032 (2023-2042)	2067 (2058-2077)
r001i1p02491	2029 (2020-2039)	2064 (2055-2074)
r001i1p02868	2035 (2026-2045)	2067 (2058-2077)

https://doi.org/10.5194/egusphere-2023-1816
Preprint. Discussion started: 18 August 2023

15 Figures

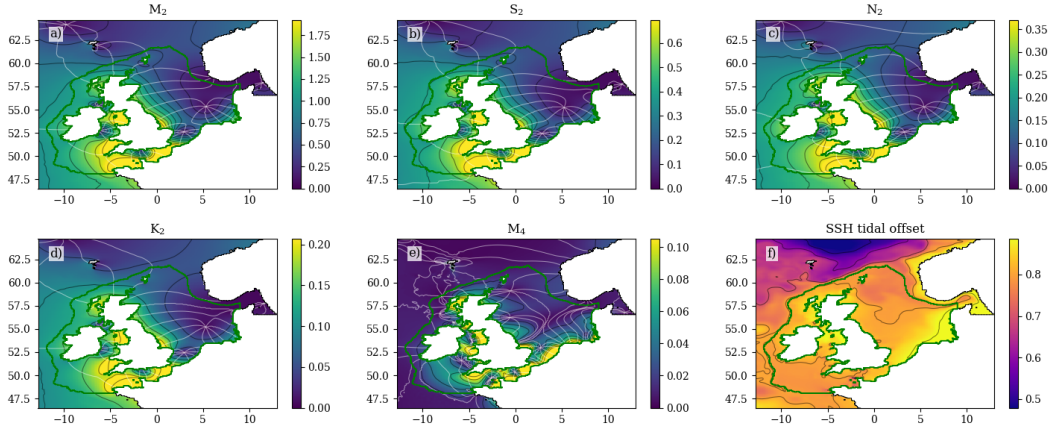

Figure 1 The (2000-2019) ensmeble mean Co-tidal chart for the 4 largest constituents (a) M_2; b) S_2; c) $N_{2;}$ and d) K_2), e) the shallow water component (M_4); and f) the offset (mean sea level). Amplitude (m) is represent by the colour map, with black contours matching the colorbar tick labels. The grey contours give the phase in 45° intervals.

https://doi.org/10.5194/egusphere-2023-1816
Preprint. Discussion started: 18 August 2023

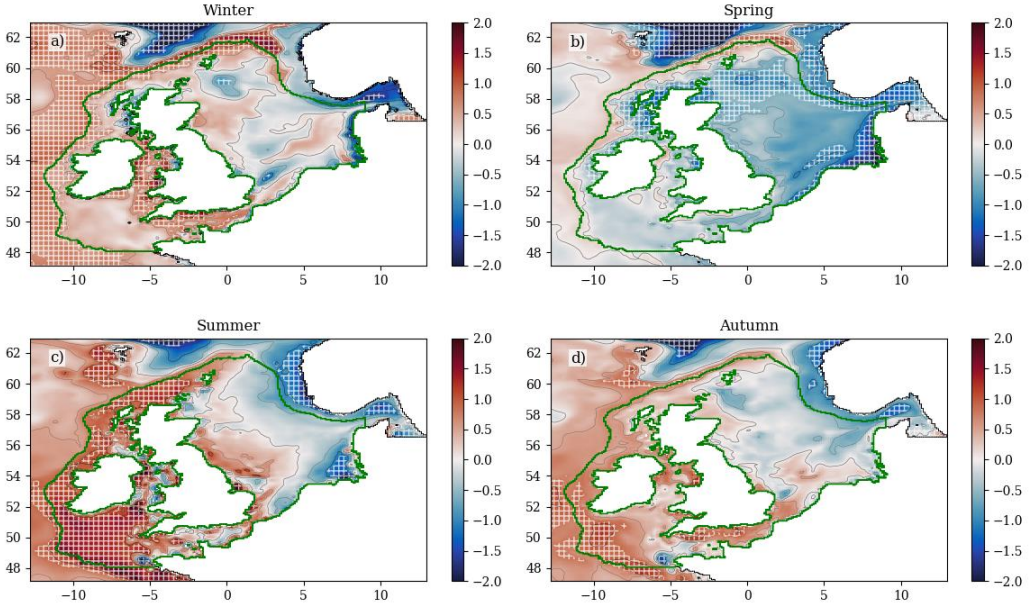

1135

Figure 2 SST bias of the PPE Ensemble mean for 2000-2019 (for the 4 seasons) compared to the OSTIA SST. The hatching shows where the OSTIA SSTs is more than 1.96 (ensemble) standard deviations from the ensemble mean.

https://doi.org/10.5194/egusphere-2023-1816
Preprint. Discussion started: 18 August 2023

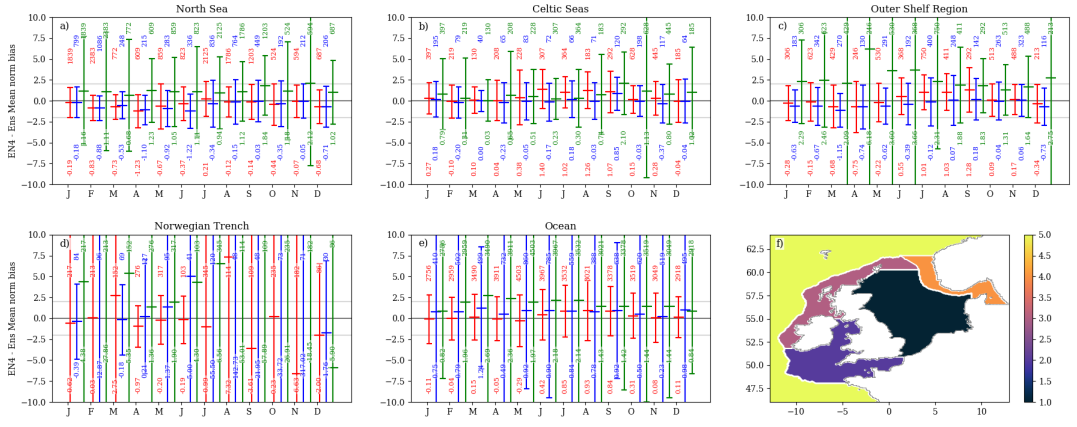

Figure 3 Regional mean distribution of normalised Model minus EN4 profile observations, for SST (red), NBT (blue) and SSS (green). Each EN4 profile – model pair is used to calculate a normalised bias (model minus ensemble mean divided by ensemble standard deviation), as shown in Figure S2-4. These data points are separated into distributions by validation regions and month – the different regions are plotted as separate subpanels, and the months are separated along the x axis (showing month number). Each distribution is plotted as the mean and ± 2 standard deviation, with 2 numbers– the number of points in each distrbution is the upper number, and the distirbution mean is the lower number. The validation region mask is giving in subpanel f, which denotes a) the North Sea; b) the Celtic Seas; c) Outer Shelf Region; d) the Norwegian Trench (and Skagerak and Kategat) and e) the oceanic regions.

https://doi.org/10.5194/egusphere-2023-1816
Preprint. Discussion started: 18 August 2023

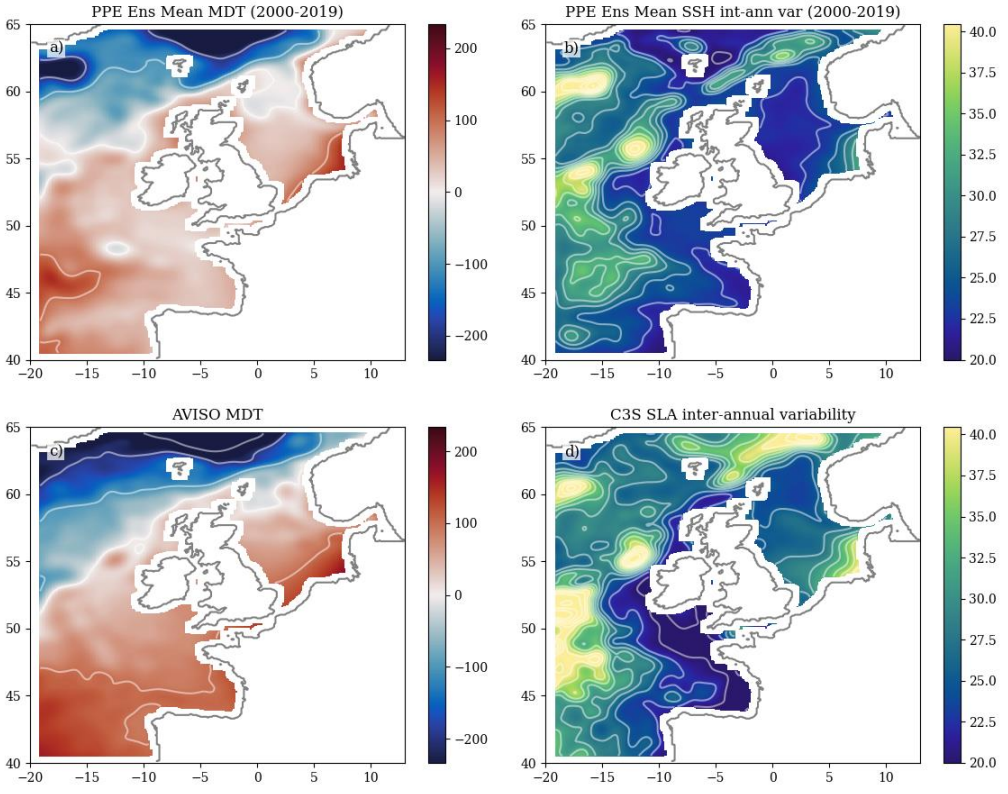

Figure 4 Comparison of Modelled SSH with satellite altimetry (mm). a) Ensemble mean SSH anomaly (2000-2019) b) Ensemble interannual variability (standard deviations of annual mean SSH, averaged over the ensemble, 2000-2019), c) AVISO MDT (mean SSH), d) CS3 interannual variability of Sea Level Anomaly.

https://doi.org/10.5194/egusphere-2023-1816
Preprint. Discussion started: 18 August 2023

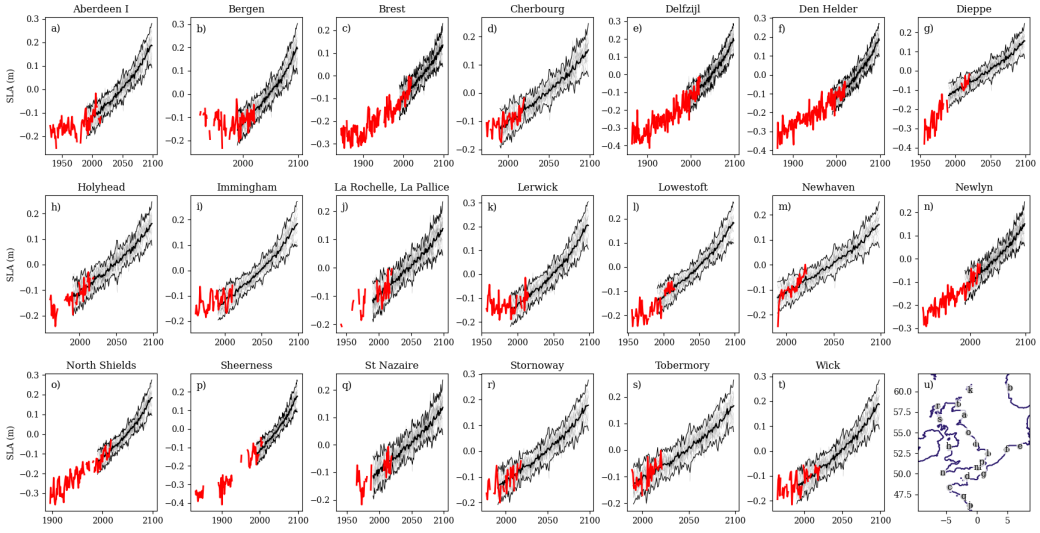

Figure 5 Tide gauge - model sea level anomaly comparison (metres). a-t) time series of annual mean SSH from tide gauges (red), and the 12 ensemble members (grey), with the ensemble mean ± 2 ensemble standard deviations shown in black. No account is taken of the differing bench marks between the model and the tide gauges, so an arbitrary offset is added to align the two datasets to allow visual comparison of the trends and variability. Note the differing time tide gauge record length leads to different ranges on the x and y axes. u) Tide gauge locations are given in Table 4.

https://doi.org/10.5194/egusphere-2023-1816
Preprint. Discussion started: 18 August 2023

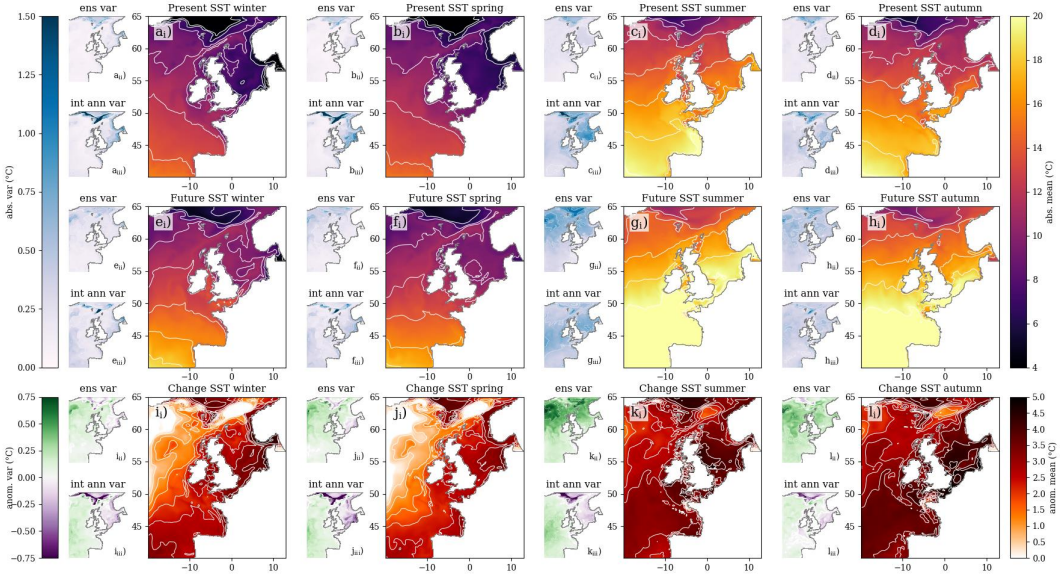

1170 **Figure 6 The early-century (2000-2019, upper row, a-d) and late-century (2079-2098, middle row, e-h) SST and their difference (bottom row, i-l). The four main columns give the seasons (winter: December-February (a, e, i); spring March-May (b, f, j); summer June- August (c, g, k); autumn September- November (d, h, l)). For each column and row, the main panel gives the ensemble mean (i), while the smaller panels on the left give the ensemble and interannual variability (upper (ii) and lower row (iii) respectrively).**

https://doi.org/10.5194/egusphere-2023-1816
Preprint. Discussion started: 18 August 2023

1175

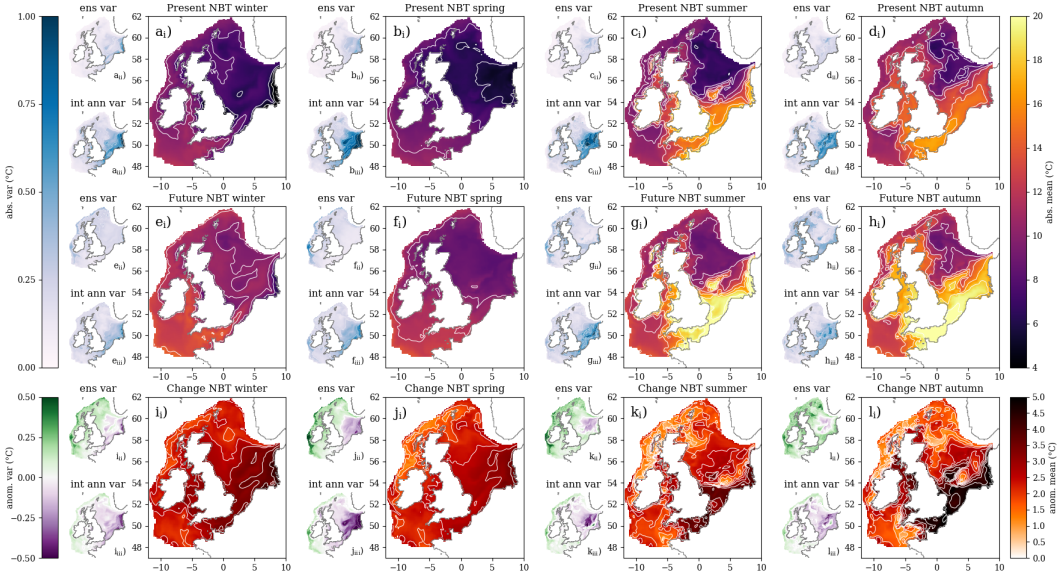

Figure 7 The early-century (2000-2019, upper row) and late-century (2079-2098, middle row) NBT and their difference (bottom row). See Figure 6 for details.

1180

https://doi.org/10.5194/egusphere-2023-1816
Preprint. Discussion started: 18 August 2023

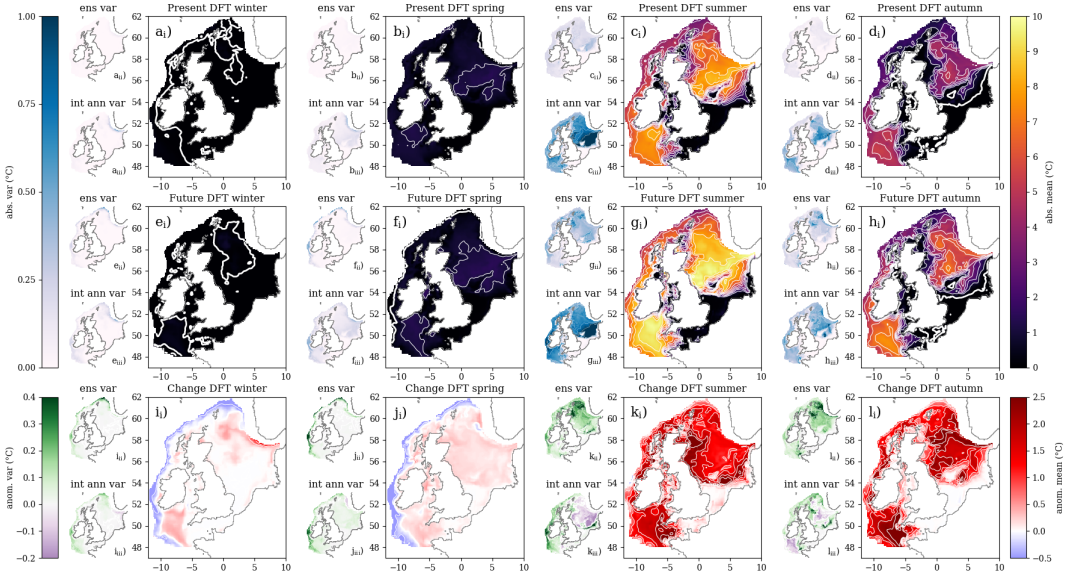

Figure 8 The early-century (2000-2019, upper row) and late-century (2079-2098, middle row) DFT and their difference (bottom row). See Figure 6 for details.

https://doi.org/10.5194/egusphere-2023-1816
Preprint. Discussion started: 18 August 2023

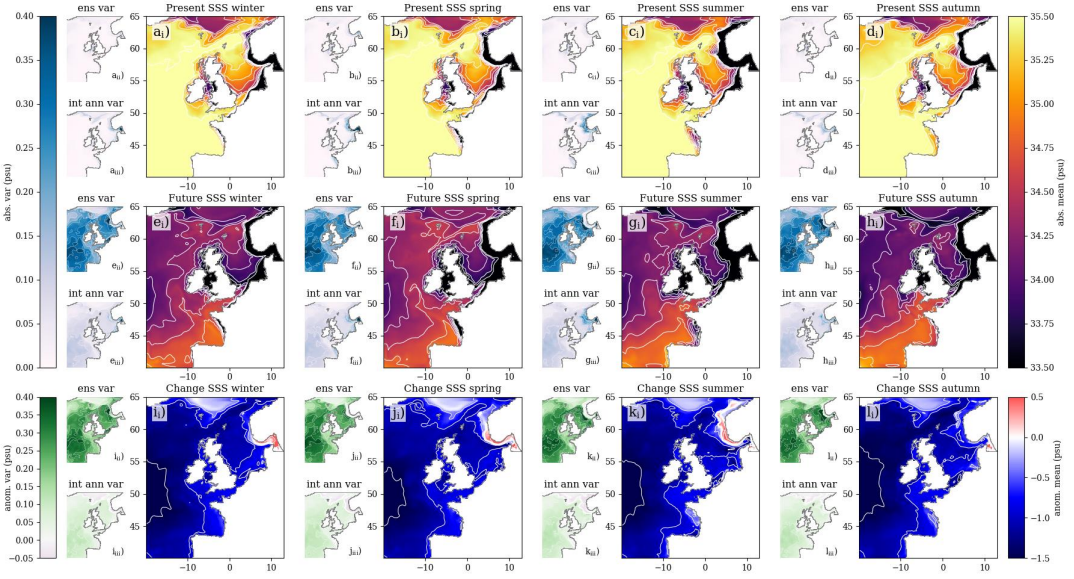

1190 **Figure 9 The early-century (2000-2019, upper row) and end-of-century (2079-2098, middle row) SSS and their difference (bottom row). See Figure 6 for details.**

https://doi.org/10.5194/egusphere-2023-1816
Preprint. Discussion started: 18 August 2023

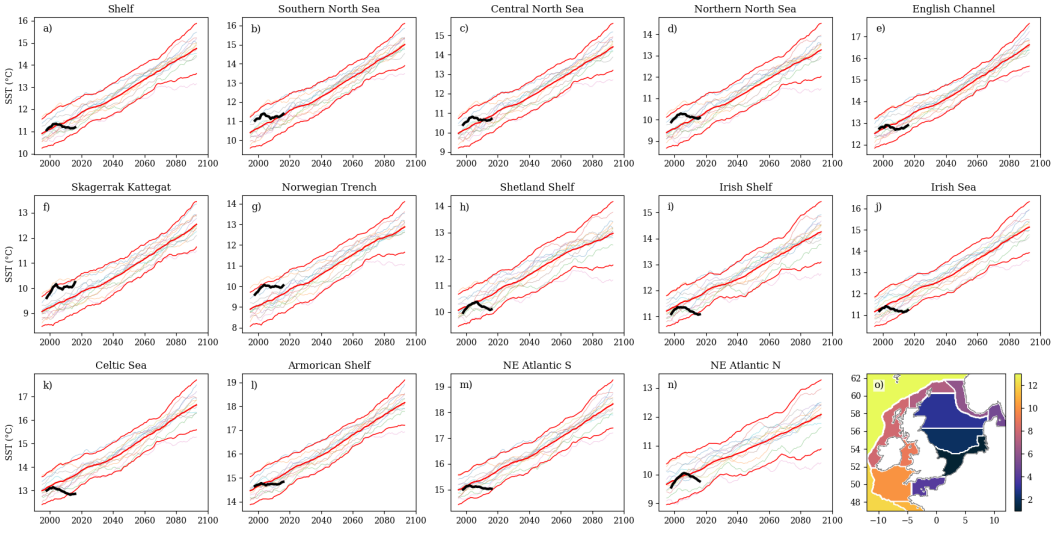

1195

Figure 10 Temporal evolution of the regional mean annual SST. Each region is given in a separate sub-panel (a-n), with o) showing the NWS region mask. Each ensmble member is filtered with a 5-year low-pass filter (shown faintly), with the ensemble mean, and ± 2 standard deviations shown in red (both based on the filtered ensemble members). The Copernicus Marine RAN reanalysis regional mean SST (also filtered) is shown in black for comparision. The y-axis limits change with each region.

1200

https://doi.org/10.5194/egusphere-2023-1816
Preprint. Discussion started: 18 August 2023

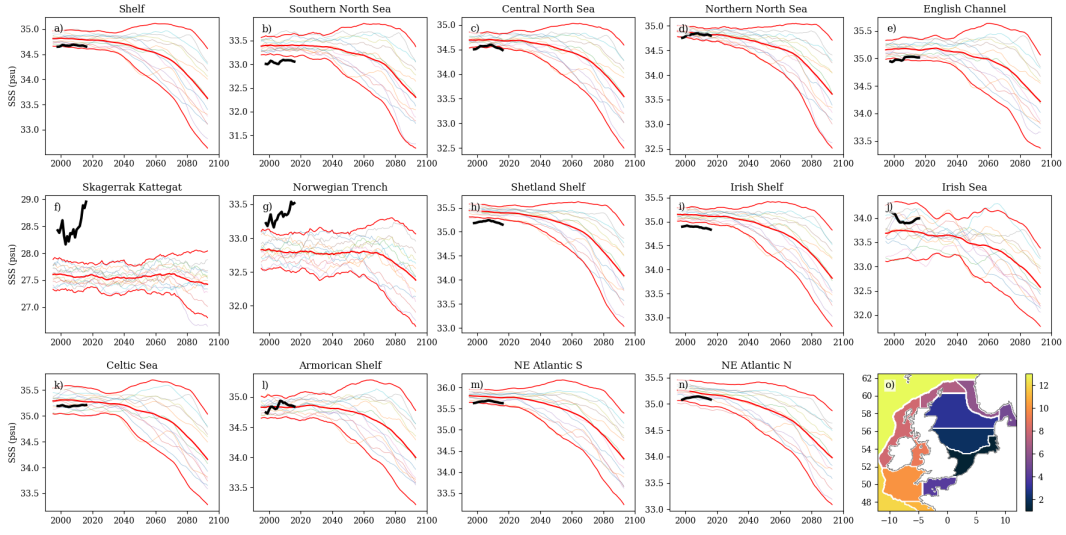

Figure 11 as Figure 10 but for SSS.

1205

https://doi.org/10.5194/egusphere-2023-1816
Preprint. Discussion started: 18 August 2023

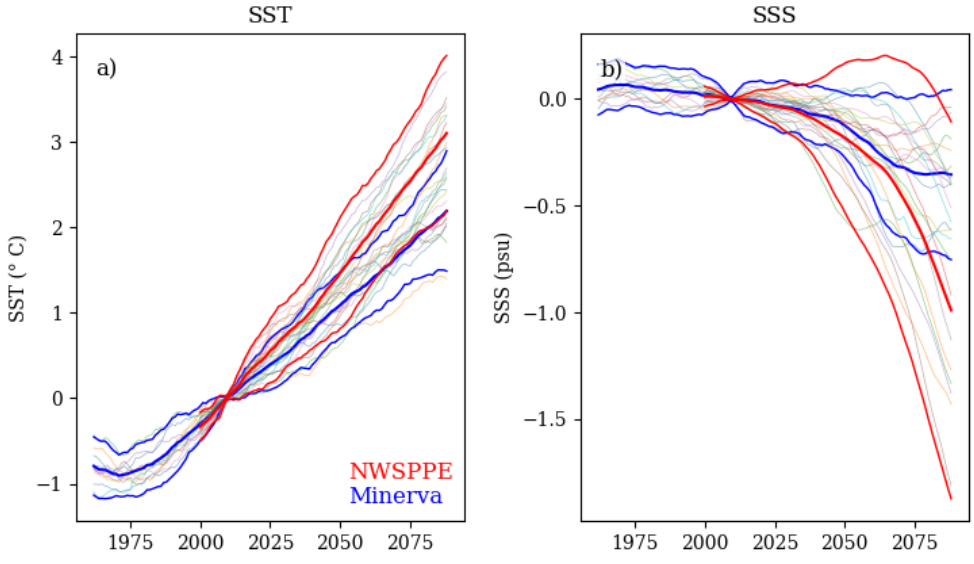

Figure 12 Comparison of a) the SST anomaly and b) SSS anomaly of the current NWSPPE ensemble (red) with the Minerva Projections (blue), for the NWS. Each ensemble member is filtered, and the 2000-2019 mean is removed, to give the anomaly. Note the current ensemble is run under rcp85, which Minerva was run under SRES A1B.

https://doi.org/10.5194/egusphere-2023-1816
Preprint. Discussion started: 18 August 2023

16 Appendix A: Tides in 360-day Calendar

The dynamics of the NWS and other shelf seas are dominated by tides. They provide the mixing energy to seasonally mix the water column in winter and define which whether a region is mixed or stratified in the summer(Simpson and Bowers, 1981). They drive important aspects of the residual and instantaneous circulation (Tinker and Hermanson, 2021). They interact with the sediment and coastline leading to geomorphological processes (Pingree and Griffiths, 1979).

Tides are controlled by aspects of the orbits of the earth moon sun systems (Pugh, 1987). The tidal frequencies are based on 5 astronomical frequencies, including the tropical year, the sidereal day and the sidereal month (Pugh, 1987). Different combinations of these frequencies give the frequencies of the tidal constituents, such as M_2 and S_2 that dominate in most regions (Pugh, 1987). The addition of these terms, and the beating between them, lead to important behaviours, including the spring-neap cycle, and the equinoctial tides (Pugh, 1987).

Climate models use a variety of calendars. In addition to the Gregorian (365+leap years) calendar, other common calendars include the 365 day with no leap year calendar, and the 360-day calendar. The 360-day calendar is made up of twelve 30-day months which make post processing, and calculation of monthly and seasonal means much simpler. However, the 360-day calendar is not directly compatible with the astronomical constants of the real world. This is not very important from the climate modellers point of view, as most current climate models do not have tides - from a global climate perspective, realistic, dynamic tides are not particularly important, and their role can generally be performed by a mixing parameterisation (Tinker et al., 2022). It becomes a problem when climate models are dynamically downscaled for shelf seas regions (e.g. Holt et al., 2010; Tinker et al., 2016). As global climate models advance, tides will become increasingly integrated, and then this may also become a problem with GCMs.

When running a shelf seas model with a 360_day calendar, the default approach (used within NEMO) is to reset the tides at the beginning of every month, so the equinoctial tides always occur at the correct time of the year (hereinafter “reset”, see Table A1). However, this introduces a jump in the tides as days are repeated of skipped (for non-30-day months), which could introduce noise into the system, and renders tidal analysis (based on least squares multiple linear regression) useless. Another approach is to convert the 360-day model forcings into 365 and to make use of the standard Gregorian calendar. This is typically achieved by repeating days, or interpolating (through time) to stretch the forcings. Both have drawbacks, including affecting the speed of synoptic systems. Another approach is to run the tides continuously from the start of the run (on their Gregorian calendar) and accept that they will become out of sync with the model running on the 360_day calendar, gaining ~5 days every year (hereinafter “drift”, see Table A1). This means that the equinoctial tides drift through the year. A final approach is to adjust the astronomical frequencies, and so the tidal constituent frequencies, to match a 360-day year, which correctly fixes the equinoctial tides to a point in the year (hereinafter “compress”, see Table A1). Each of these approaches have strengths and weaknesses, which may influence the simulations. Here we describe the three tidal implementations (reset, drift, and compress) and their effect on the tidal characteristics of the NWS. We do not assess the modification of the atmospheric and oceanic forcings.

We first give brief overview of relevant aspects of tidal theory, how the astronomical constants may be adjusted for the 360-day year, and the impact of this on the tidal constituent periods, and the important beating frequencies. We then assess the impact of this tide in a model simulation, and compare to the other methodologies.

For the NWSPPE and PDCtrl, we take a conservative approach and use the “drift” method, following Holt et al., (2010) and Tinker et al., (2016).

https://doi.org/10.5194/egusphere-2023-1816
Preprint. Discussion started: 18 August 2023

16.1 Method

16.1.1 Tidal theory

Here we give a brief overview of relevant aspects of tidal theory, mainly taken from Pugh (1987).

Harmonic expansion of the tide breaks it into many sinusoidal constituents with astronomically defined frequencies, and amplitudes and phases that vary with space. For a given location, the effect of the tide on the sea level can be defined as:

$$\eta = \sum \; a_n \sin(\sigma_n t + \phi_n) + \eta_0 \qquad (A1)$$

Where a η is the sea level (and η_0 is the mean sea level), and for constituent n, a_n is the amplitude, σ_n is the frequency ($2\pi/T$ where T is the tidal period), and ϕ_n is the phase. The a_n and ϕ_n can be found with least squares multiple linear regression (Pugh, 1987).

There are a number of important astronomical frequencies that define the frequencies of the tidal constituents: the mean solar day ($\omega_0 = 2\pi/1$ day = $2\pi/24$hr); the mean lunar day ($\omega_1 = 2\pi/1.0351$ day = $2\pi/24.8424$hr); the sidereal month ($\omega_2 = 2\pi/27.3217$ day = $2\pi/655.7208$); the tropical year ($\omega_3 = 2\pi/365.2422$ day = $2\pi/8765.8128$ hr); moon's perigee ($\omega_4 = 2\pi/8.85$ years); the regression of the moon's nodes ($\omega_5 = 2\pi/18.61$ years); and the perihelion ($\omega_6 = 2\pi/20942$ years).

The tidal constituent frequencies (ω_n) can be calculated as:

$$\omega_n = i_1\omega_1 + i_2\omega_2 + i_3\omega_3 + i_4\omega_4 + i_5\omega_5 + i_6\omega_6 \qquad (A2)$$

where i_1, i_2, i_3… are small integers ($|i|<5$). The use of both the solar and lunar days is not necessary as $\omega_0 = \omega_1 + \omega_2 - \omega_3$. The species of the constituent is defined by i_1 (i_1 = 2 semi-diurnal, = 1 diurnal; 0, long period) (Pugh, 1987). Doodson notation concisely describes the tidal constituents: i_2-i_6 are incremented by 5 (so there are no negative integers); i_1-i_6 are combined into a single number. For example, M_2 has a Doodson number of 255.555 ($i_1 = 2$, $\omega_n = 2\omega_1$), S_2 is 273.555 ($i_1 = 2$, $i_2 = 2$, $i_3 = -2$, $\omega_n = 2\omega_1 + 2\omega_2 - 2\omega_3$), and K_2 is 275.555 ($i_1 = 2$, $i_2 = 2$, $\omega_n = 2\omega_1 + 2\omega_2$),

When two tidal constituents of slightly different frequencies are added together, they beat as they come in and out of phase. The M_2 and S_2 constituents beat to give the spring neap cycle, and the S_2 and K_2 constituent beat to give the equinoctial tides. The beat envelope function is:

$$\pm\left[a_1 + a_2\left[\cos\left((\sigma_1 - \sigma_2)t + (\phi_1 - \phi_2)\right)\right]\right] \qquad (A3)$$

where the constituents are ordered by amplitude size (i.e. $a_1 > a_2$). This gives the beat frequency (σ_1-σ_2) and phase (ϕ_1-ϕ_2), so the M_2-S_2 spring neap cycle has a frequency of $2\pi/12.42 - 2\pi/12$ = 354.85 hr = 14.7 days, and the S_2-K_2 has a beat frequency of 182.6221 days.

You can also calculate the beat frequencies from the Doodson numbers. For example, the difference between M_2 and S_2 is 255.555 and 273.555 implies a difference in frequency of ($\omega_n = 2\omega_2 - 2\omega_3$), while S_2 and K_2 is 273.555 and 275.555 is ($\omega_n = -2\omega_3$).

16.1.2 "Compress" tidal scheme.

We introduce a tidal scheme where one of the astronomical frequencies modified to the 360-day year. The frequency of the tropical year (ω_3) is modified to $2\pi/360$days = $2\pi/8640$hr. This has no impact on the S_1 or S_2 tidal frequencies but reduces the M_2 period by 1.84 seconds. The impact on the beat frequencies is larger, with the spring neap cycle increasing from 14 days 18hr 22 mins to 14 days and 18 hr 47 mins, and the equinoctial tidal frequencies decreasing from 182.621 days to 180 days, exactly half a 360-day year.

We have implemented this scheme in the shelf seas model NEMO Coastal Ocean model 9 (CO9, NEMO version 4.0.4), and will assess the impact of this of the simulation of the tides. Note that we have not used this scheme in the NWSPPE.

https://doi.org/10.5194/egusphere-2023-1816
Preprint. Discussion started: 18 August 2023

16.1.3 Models and Experimental Design

We use the Nemo version 4.04, Coastal Ocean model version 9 (O'Dea), run on the 7km NWS domain (Atlantic Margin Model 7km - AMM7), in a set of 40-year simulations with the different approaches to modelling the tide (see Table A3). We use these simulations to investigate the impact of the different tidal schemes on the resulting emergent tidal behaviour. We assess these runs for their amphidromic systems, and distribution of amplitude and phase of the different tidal constituents. We also pay particular attention to the difference in amplitude and phase between key constituent pairs, as this controls the behaviour of their tidal beats, which is a particular weakness of some of the tidal schemes We do not assess the impact on other oceanic properties (such as temperature),which is likely to be more subtle, and require longer simulations to investigate.

We assess the second 20-year period is used in this assessment, as this ties in with the inline tidal harmonic analysis within NEMO (within DIA/diaharm_fast.F90, within https://github.com/hadjt/NEMO_4.0.4_CO9_shelf_climate/tree/master/src/OCE/).

16.1.4 NEMO model code

Most of the code added to NEMO is within SBC/tide_mod.F90 (https://github.com/hadjt/NEMO_4.0.4_CO9_shelf_climate/blob/master/src/OCE/SBC/tide_mod.F90). This allows the user to choose between the three tidal schemes using the `nam_tides360` namelist, and the `ln_tide_drift` and `ln_tide_compress` logical keywords.

16.1.5 Analysis techniques: Least Squares tidal harmonic analysis

We use a tidal harmonic analysis based on a least-squares method to calculate the phase and amplitudes of the tidal constituents as described by Pugh (1987). This method considers the tidal signal as:

$$T(t) = Z_0 + \sum_N H_n f_n cos\left[\sigma_n t - g_n + (V_n - u_n)\right] \qquad (A4)$$

where the Z_0 is the mean sea level, H_n and f_n are the amplitude and the nodal factor for the n^{th} tidal constituent, t is time σ_n is the tidal frequency g_n is the tidal phase, and V_n and u_n are the phase angle at time zero and the nodal angle respectively. t and the terms f_n, σ_n, V_n and u_n are known *a priori*, as is the surface elevation $T(t)$. (A4) is solved for Z_0, H_n, g_n by using a least-squares estimation.

This is done online by NEMO (see https://github.com/hadjt/NEMO_4.0.4_CO9_shelf_climate/blob/master/src/OCE/DIA/diaharm_fast.F90) using consecutive 20 year periods of the model simulation. We use the second 20-year period to avoid any spin-up issues.

One issue of the standard NEMO tide configuration ("reset") is that the time counter jumps at the end of 360-day calendar months for months that should have 31 days (or February). NEMO's online harmonic analysis code takes account of this, as both the tide, and the time counter jump. We have written python code that replicate the NEMO online harmonic analysis code. We can then to see how these jumps affect the tidal analysis, if not taken into account – i.e. if someone simply analysed the hourly sea surface height model output. This is used in Figure A2c (c.f. Figure A2b) which shows very large errors, and (not shown) a near zero M_2 amplitude, and larger S_2 amplitude.

16.2 Results

16.2.1 Harmonic analysis

We fit a least square tidal fit to the data (Figure A1). We use the RMSE of the residuals to quantify how well the data is fit (Figure A2). As the tides see discontinuous time for Reset, with days repeated and missing - we carefully recreate the time array for its tidal analysis, otherwise the most diurnal constituents (including M_2) appear to be S_2. We include the RMSE when

https://doi.org/10.5194/egusphere-2023-1816
Preprint. Discussion started: 18 August 2023

this is not done, see Figure A2c, which shows an ~ 10-fold increase in RMSE. Generally, all models have similar RMSE, which are small compared to the tidal range, and so we can use the computed phase and amplitudes for the rest of the study.

The locations of the amphidromes are insensitive to the simulation. The difference of the amplitudes between the simulation is typically less than 5%. The phases of the Compress experiment have the largest difference.

The phase of individual diurnal and semidiurnal constituents is not thought to be of any particular importance as the peak will move through the day (apart from S_1, S_2 – hence spring HW is always at the same time). However, the phase difference between constituents give the phase of the tidal beats, which can be important, and can occur at the same time of the year.

16.2.2 Important beat frequency and amplitude

To identify the important beat frequency pairs, we use (A3) to find the beat frequency of each pair of constituents, and their amplitude (a_2 in (A3), i.e. the smaller of the two amplitudes) for the shelf mean (Figure A4). We focus on beat pairs with periods greater than 100 days. Figure A4 shows that the S_2-K_2 pair are the dominant biannual beat pair, with K_1-P_1 playing a secondary role. The annual beat frequencies are much weaker, with the S_2-T_2 pair dominating, and K_1-S_1 and P_1-S_1 having a lessor *(and similar)* role. K_2-T_2 is triannual, while N_2-NU_2 and $2N_2$-MU_2 occur every 202 days and 10hr20min, and 202 days 13hr35min respectively.

Figure A4 and Table A4 show that the proposed "compress" tidal system correctly adjusts the beat frequencies to the 360-day year, however the phase of the beat is also important – it is what makes the equinoctial tides occur during the equinoxes. We can use (A3) to find the beat phase (the difference between the individual tidal constituent phases) and calculate the timing of the peak of the beats - we use this to show how well the different tidal systems reproduce the phase of the beating waves.

Figure A5 shows that Gregorian and the reset have the same timing of the maxima. The drift can be seen to drift throughout the period, progressing ~5 days per year. Compress is comparable to Greg and Reset, showing that it is capable of reproducing the period and timing of the tidal beats. We can look at the maps of the spatial patterns of the timing of the beat pair maximum (Figure A6). For the most important pair (S_2-K_2), the patterns of the timing agree visually, and the timing is within ~10 days, which is considered reasonable.

16.3 Conclusions

We have compared the ability of different 360-day tidal schemes to simulate the emergent behaviour of the NWS tides from simulation with the standard Gregorian calendar. We base our analysis on the results of a least squares tidal harmonic analysis. This has to be modified for two tidal schemes (using the modified tidal periods for Compress, and using a synthetic time for Reset).

Reset is the standard tidal scheme within NEMO, but leads to jumps within the tide at the end of the month. This changes the average M_2 period, and so the errors associated with the (uncorrected) harmonic analysis are much higher (Figure A2c).

With the corrected the harmonic analysis, all 360-day tidal schemes simulate the co-tidal charts of the control (Greg) well (Figure A1) with a similar (pattern and magnitude of) RMS errors (Figure A2). This is the most important quality, and each scheme performs equally well.

The beat phases give the timings of the equinoctial tide. Both Reset and Compress simulate the correct timings, whereas the Beat Period doesn't match the 360-day calendar, so even if the phase is correct, the timings drift through the calendar each year, typically gaining 5 days every year.

For both these criteria, the Compress tidal scheme performs well, and no other scheme out performs it. However, it is unpublished, and some users may be impacted by some of its features (M_2 tide shortened by 2 second, Spring-Neap cycle increases by 25 minutes). We therefore use the Drift tidal scheme in our projections, as it has been used in earlier projections (e.g. Holt et al., 2010; Tinker et al., 2016), and is more conservative choice.

https://doi.org/10.5194/egusphere-2023-1816
Preprint. Discussion started: 18 August 2023

16.4 Appendix Tables

Table A1 360-day tide methodologies, and their advantages and disadvantages.

Methodology	Advantages	Disadvantages
Reset	Default methodology in NEMO Equinoctial Tides at correct time of the year.	Tidal boundaries are discontinuous at end of months that do not only have 30 days. This, on average, significantly changes the period of the M_2 (and other) tidal constituents. This renders standard tidal harmonics analysis ineffective.
Drift	Allows a continuous stimulation of the tides. Doesn't modify the periods of the tidal constituents. Standard Tidal analysis is applicable.	Equinoctial Tides occur ~5 days earlier every year.
Compress	Allows a continuous stimulation of the tides. Standard Tidal analysis is applicable when using modified tidal constituent periods Equinoctial Tides occur at correct time of the year.	Slightly modifies the periods of the tidal constituents, following the calculations described in this paper. New methodology, not used in published studies. Impact of modifications on all end users not known.
Modification of the atmospheric and lateral oceanic forcings to fit the Gregorian calendar (included here as a control)	Tides are not modified at all.	Different methodologies well have different implications. Temporal interpolation of the atmospheric conditions or skipping/repeating day will affect the passage of synoptic systems. This may affect surface momentum, heat and water fluxes, which could lead to systematic biases in the simulated climate. In our Gregorian, we skip/repeat days.

1370

https://doi.org/10.5194/egusphere-2023-1816
Preprint. Discussion started: 18 August 2023

Table A2 Period of updated tidal constituent

Constituent (Darwin symbol)	Species	Doodson number	Period	New Period	Difference
M_2	Principal lunar semidiurnal.	255.555	12.421 hr	12.420 hr	-1.845 sec
S_2	Principal solar semidiurnal.	273.555	12.000 hr	12.000 hr	0.000 sec
N_2	Larger lunar elliptic semidiurnal.	245.655	12.658 hr	12.658 hr	-1.916 sec
K_2	Lunisolar semidiurnal.	275.555	11.967 hr	11.967 hr	-1.713 sec
K_1	Lunar diurnal.	165.555	23.934 hr	23.934 hr	-3.426 sec
NU_2	Larger lunar evectional.	247.455	12.626 hr	12.625 hr	-3.813 sec
O_1	Lunar diurnal.	145.555	25.819 hr	25.818 hr	-3.987 sec
L_2	Smaller lunar elliptic semidiurnal.	265.455	12.192 hr	12.191 hr	-1.778 sec
$2N_2$	Lunar elliptical semidiurnal second-order.	235.755	12.905 hr	12.905 hr	-1.992 sec
MU_2	Variational.	237.555	12.872 hr	12.871 hr	-3.963 sec
T_2	Larger solar elliptic.	272.555	12.016 hr	12.017 hr	0.864 sec
M_4	Shallow water overtide of principal lunar.	455.555	6.210 hr	6.210 hr	-0.923 sec
Q_1	Larger lunar elliptic diurnal.	135.655	26.868 hr	26.867 hr	-4.317 sec
P_1	Solar diurnal.	163.555	24.066 hr	24.067 hr	3.464 sec
S_1	Solar diurnal.	164.555	24.000 hr	24.000 hr	0.000 sec

https://doi.org/10.5194/egusphere-2023-1816
Preprint. Discussion started: 18 August 2023

1375

Table A3 Name and description of simulations

Name	Description
Greg	360-day forcings are used to run a 360-day simulation. The last days of February forcings have been removed, and the forcings of the 30th have been repeated where necessary
Reset	The tides are reset to the Gregorian calendar at the beginning for every day (using the day, month, year, and allowing non-existent days to continue into the next month if necessary. This is the standard implementation within NEMO. A Least-Square's tidal analysis does not work directly, but can be used by converting the 360-day calendar dates to the Gregorian calendar (e.g. 25th Feb - 30th Feb and 1st - 2nd Jan – becomes 25th-28th Feb and 1st - 4th Jan.).
Reset (uncorrected)	The same as Reset, but without the correction to the dates into Gregorian calendar.
Drift	Run the Gregorian tides on the days since 1st January 1900, and then convert these to the 360-day calendar
Compress	Run with the updated tidal constituent periods.

https://doi.org/10.5194/egusphere-2023-1816
Preprint. Discussion started: 18 August 2023

Table A4 Periods of beat pairs

Constituent Pair	Gregorian Period (days)	360-day Period (days)
S_2-T_2	365.26	360.01
K_1-S_1	365.24	360.00
P_1-S_1	365.25	360.00
S_2-K_2	182.62	180.00
K_1-P_1	182.62	180.00
N_2-NU_2	205.89	202.57
$2N_2$-MU_2	205.89	202.57
K_2-T_2	121.75	120.00

https://doi.org/10.5194/egusphere-2023-1816
Preprint. Discussion started: 18 August 2023

16.5 Appendix Figures

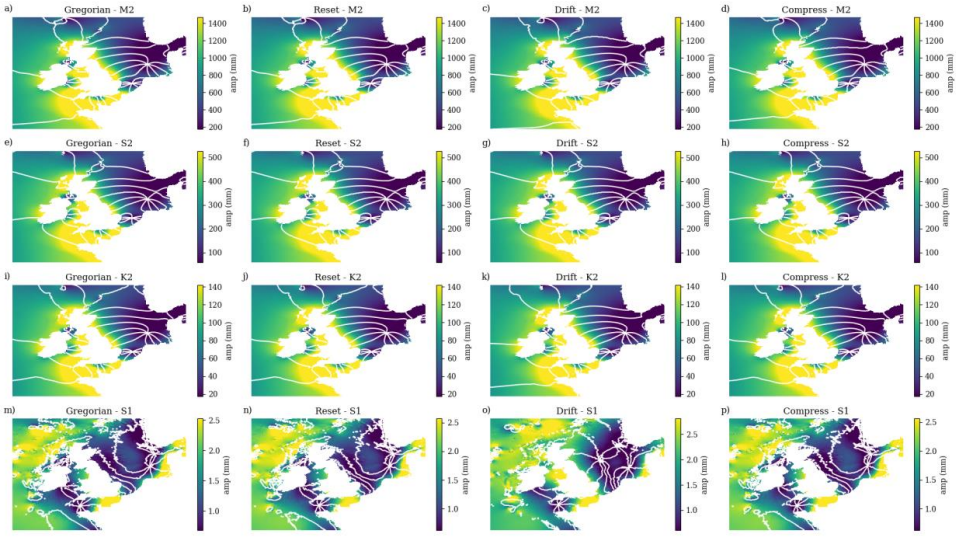

Figure A1 Cotidal charts for the M_2 (a-d), S_2 (e-h), K_2 (i-l) and S_1 (m-p) tidal constituents under the Gregorian (control, a, e, i, m), Reset (b, f, j, n), Drift (c, g, k, o) and Compress (d, h, l, p) tidal schemes. The colour maps represent the amplitude, and is constant for a given constituent, while the lines are lines of equal phase, (every 45°).

https://doi.org/10.5194/egusphere-2023-1816
Preprint. Discussion started: 18 August 2023

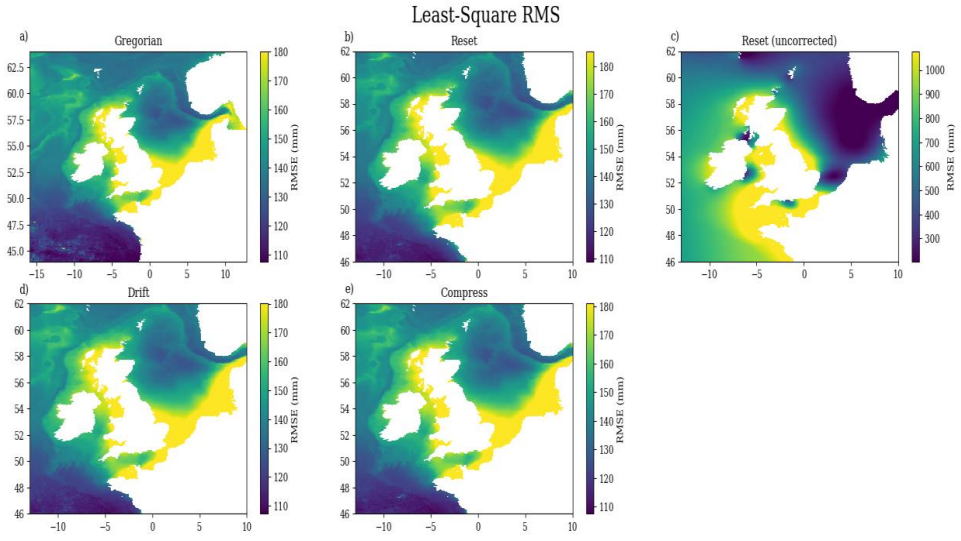

1395

Figure A2 RMS of least square tidal fit, for the simulations: a Gregorian; b Reset; c Reset (uncorrected); d Drift; and e Compress. For Reset, we construct an equivalent time (resetting to the Gregorian calendar at the beginning of each month) and use this for the least squares. We do not correct this in Reset (uncorrected), and the RMS errors are much greater (c).

https://doi.org/10.5194/egusphere-2023-1816
Preprint. Discussion started: 18 August 2023

1400

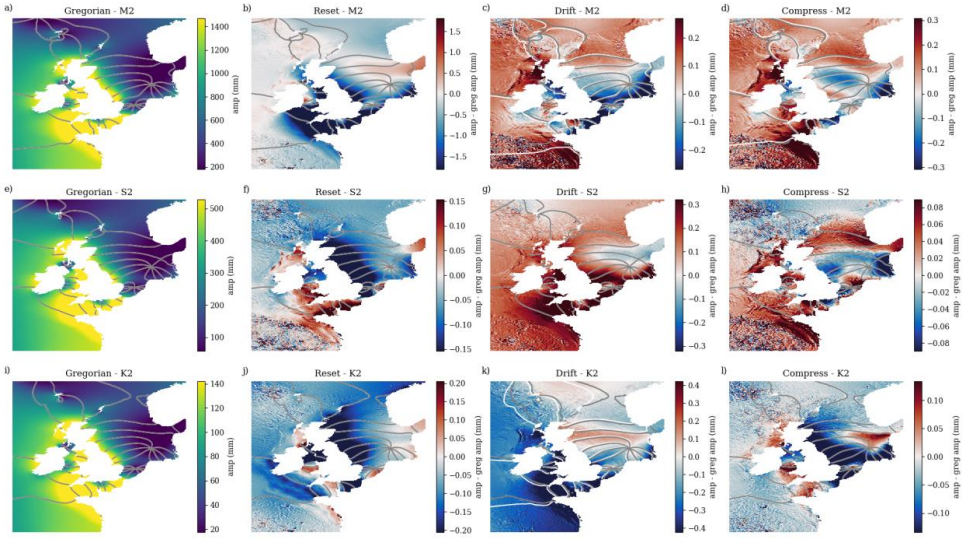

Figure A3 Cotidal charts for M_2, S_2 and K_2 (upper, middle, and lower row respectively), for Gregorian (left column) and anomalies (relative to Gregorian) for Reset, Drift and Compress (second, third and fourth column respectively). The colours give the amplitude (or amplitude minus Gregorian amplitude anomaly) in mm, the contours give the co-phase lines (every 45 degrees), grey for Gregorian, and white for Reset, Drift and Compress respectively.

1405

https://doi.org/10.5194/egusphere-2023-1816
Preprint. Discussion started: 18 August 2023

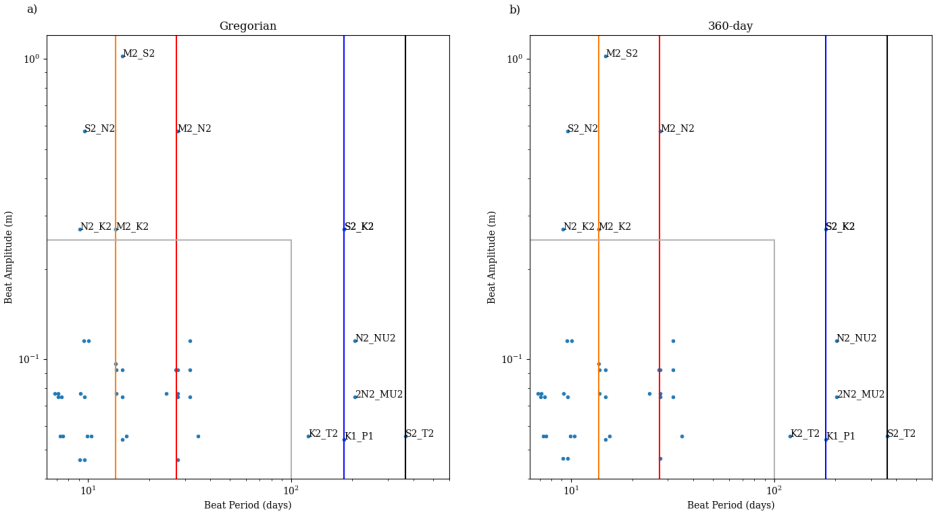

1410

Figure A4 Beat frequency and amplitude for the standard Gregorian tidal constituent frequencies (left), and the modified 360_day frequencies under the Compress tidal scheme (right). the yellow and red lines show the monthly, and bimontly frequecies, and the blue and black lines show the biennial and annual frequencies ($2\pi/(365.24x24)$ and $2\pi/(360x24)$ respectively). The grey box shows the beat pairs with periods less than 100 days, and ampitudes less than 0.2m.

1415

https://doi.org/10.5194/egusphere-2023-1816
Preprint. Discussion started: 18 August 2023

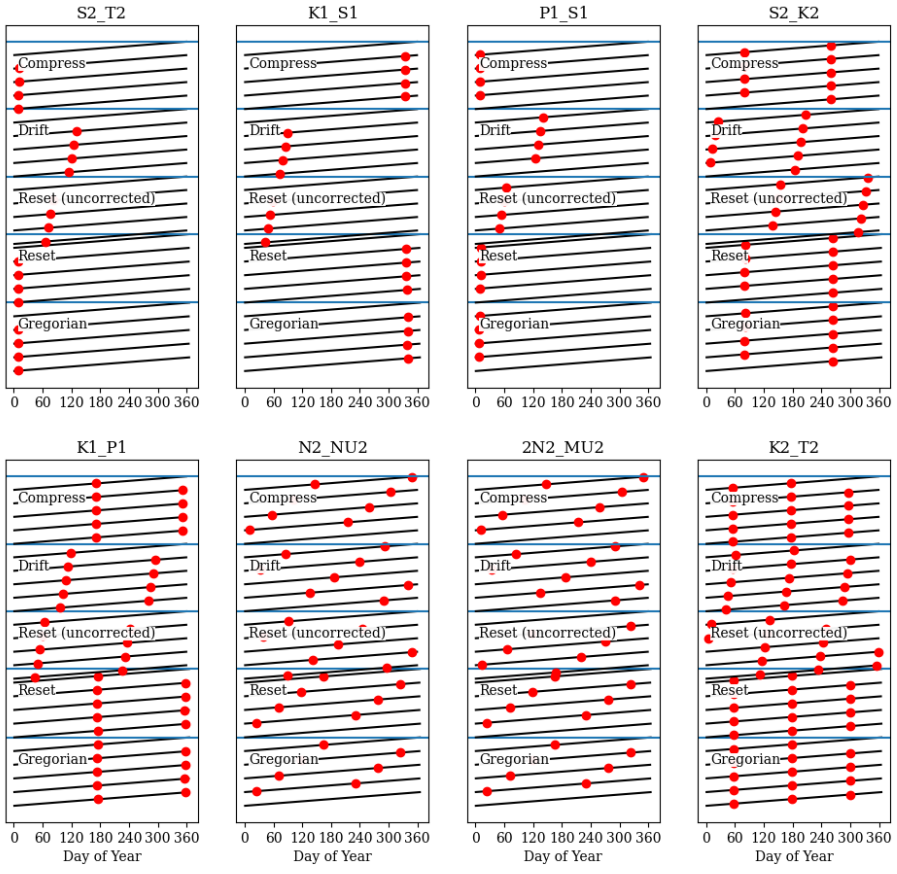

Figure A5 The timing (day of year) of the maximum of the beating tidal constituent pairs (with periods greater than 100 days) for the four different tidal systems for an example location. Each subplot is a beating tidal pair. The black line represents the day of the year (in the x direction) and the decimal year (in the y direction). The red dot is the local maximum of the beating pair. Each tidal system (Greg, Reset, Reset (uncorrected), Drift, and Compress) is stacked on top of one another.

https://doi.org/10.5194/egusphere-2023-1816
Preprint. Discussion started: 18 August 2023

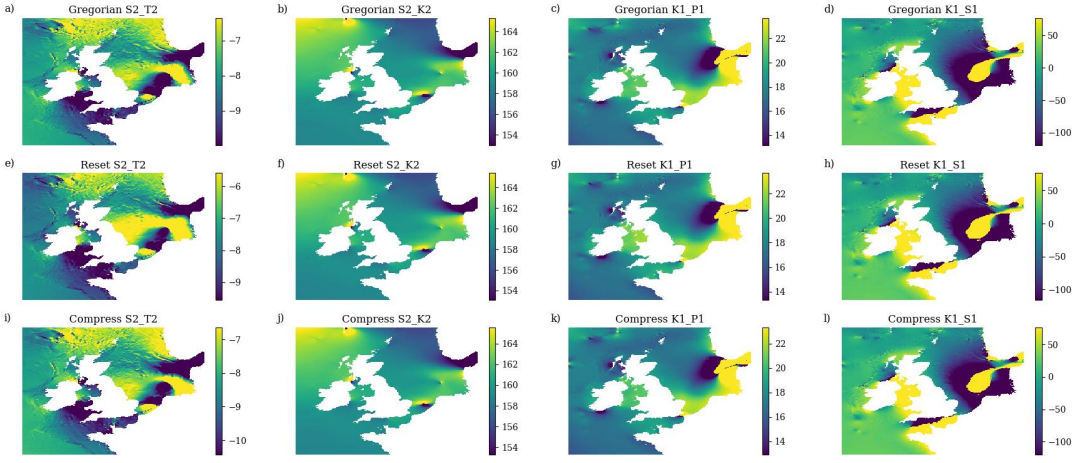

1425

Figure A6 Timing of largest beat pair maximum (in day of year), for pairs that occurs at approximately the same time of each year. Note S_2-K_2 are the beating pair with the greatest amplitude,